IEEE Access
Multidisciplinary ⋮ Rapid Review ⋮ Open Access Journal

Received November 15, 2019, accepted December 4, 2019, date of publication December 10, 2019,
date of current version December 23, 2019.

Digital Object Identifier 10.1109/ACCESS.2019.2958651

Dispatch for Urban Integrated Heat and Power System Considering Secondary PM2.5 Under Smart Environmental Sensing

SICHENG PENG[1], HONGXIA WANG[1], YUQIONG ZHANG[2], DICHEN LIU[1], (Member, IEEE), JINCHANG LI[1], AND HENGRUI MA[3], (Member, IEEE)

[1]School of Electrical Engineering and Automation, Wuhan University, Wuhan 430072, China
[2]China Electric Power Research Institute, State Grid, Beijing 100192, China
[3]Tus-Institute for Renewable Energy, Qinghai University, Xining 810016, China

Corresponding author: Hongxia Wang (2018282070092@whu.edu.cn)

This work was supported in part by the Qinghai Provincial Natural Science Foundation of China under Grant 2019-ZJ-950Q, and in part by the research funding from State Grid Corporation of China under Grant JS17-18-002.

ABSTRACT To improve the air quality and reduce the human settlement pollution, the effects of initial air pollutant emissions from urban heat and power generation with the diffusion of pollutants were often considered in the energy system dispatch, but the effects of secondary PM2.5 hazards caused by the urban energy system were almost ignored. In the urban integrated heat and power systems (UIHPS), under the support of smart environmental sensing, the introduction of integrated demand response (IDR) between the energy production side and consumer side is an effective means of reducing primary and secondary PM2.5 hazards. As for the diffusion of primary pollutants and the generation of secondary PM2.5 are affected by the uncertainty of weather conditions, a stochastic environmental economic dispatch (SEED) model for UIHPS considering IDR is proposed in this paper. Linearized secondary PM2.5 generation and diffusion functions for UIHPS dispatch are introduced into the objective function. The price-based IDR is performed on the Stackelberg game mechanism, and the game equilibrium solution is transformed as the SEED's constraint set by using the backward induction method. Simulations show that under the partly data supply from smart environmental sensing, the SEED model considering the secondary PM2.5 and IDR can effectively alleviate the comprehensive hazard of PM2.5 under severe haze weather.

INDEX TERMS Environmental-economic dispatch, integrated heat and power system, secondary pm2.5, integrated demand response, Stackelberg game.

I. INTRODUCTION

In recent years, although countries have paid more and more attention to atmospheric environmental protection, their air pollution problems are still very serious. Among them, particulate matter 2.5 micrometers or less in diameter (PM2.5) are the main cause of haze [1]–[4]. The PM2.5 pollution is caused by primary PM2.5 directly discharged by the pollution source and secondary PM2.5 generated by the reaction of various pollutants in the atmosphere. In the case of serious pollution, secondary aerosols account for a higher proportion of total PM2.5, sometimes up to 70% [5]. As the city's main fossil energy consumer and secondary energy supplier, the thermal and power industries contribute a lot to the PM2.5 concentration, which is second only to industrial production and motor vehicle emissions in autumn and winter [6]. It should be noted that in the context of the comprehensive promotion of ultra-low emission conversion of the units [7], although the initial pollutant discharge level of the units has been significantly reduced [8], the contribution of the energy system to the PM2.5 concentration is still not optimistic, which is largely caused by the secondary PM2.5. Therefore, the secondary PM2.5 generation caused by the initial emissions of thermal power plants (TPP) and the combined heat and power (CHP) plants must be taken seriously.

In particular, to improve the efficiency of energy supply, CHP units are often built in populated areas in cities. And in the smog and haze weather that is not conducive to the spread

The associate editor coordinating the review of this manuscript and approving it for publication was Honghao Gao.

of pollutants, the primary and secondary PM2.5 caused by CHP units may be more harmful to the health of residents than TPP units'. Therefore, UIHPS offers more potential to reduce PM2.5 hazards. In the deregulated energy market, production-side and user-side trading mechanisms based on the IDR can further extend this potential [9]. The introduction of trading forms such as Stackblerg game can enable multi-energy users to provide more optimization space for the system and improve their interests through the complementarity of heat and power demand, which can achieve a multi-party win-win [10], [11]. At the same time, with the continuous development of environmental sensing technology, smart environment sensing can provide a solid support for UIHPS by suppling real-time and effective human settlements and background pollutant data, to reduce the UIHPS's pm2.5 comprehensive hazard considering secondary pm2.5 by performing short-cycle dispatch [12]–[14].

Environmental Economic dispatch (EED), which aims to improve the impact of power systems on environmental pollution, is one of the research directions that researchers have paid close attention to and has been continuously developed [15]–[21]. However, limited research focuses on the role of CHP plants in pollution reduction [22]–[24]. At the same time, the existing research on the environmental benefits of the cogeneration system only considers the control of total emissions. However, the harm of PM2.5 to residents' health [25] is mainly determined by the ground level concentration (GLC). The law of the diffusion of matter in the atmosphere has a great influence on the degree of damage caused by the initial emission of PM2.5. To this end, some scholars have established a temporal and spatial distribution (TSD) model of pollutant emissions from power systems, shifting research focus from total pollutant control to optimization of GLC [26] uses the Gaussian plume diffusion model to simulate the diffusion of PM2.5 generated by the power system and incorporates it into the unit combination through differentiated environmental capacity costs. The Gaussian puff model used in [27], [28] is an extension of the Gaussian plume model, which is more suitable for small calm wind weather, and can improve the accuracy of pollutants TSD in haze weather [29] further considered the influence of atmospheric boundary layer (ABL) and attenuation benefits on pollutant dispersion, established a TSD model for various pollutants, and proposed a high-dimensional multi-objective optimization method; Based on this model, [30] developed a multi-objective EED strategy for the power-natural gas integrated energy system. However, the research using pollutant diffusion models to study the environmental benefits of CHP units has not been reported.

In addition, previous studies barely mention the control of secondary PM2.5 hazards caused by emissions from energy systems, which does not match the actual hazard level of the secondary PM2.5. Reasons for lack of research in this field may include: (1) The composition and mechanism of the secondary PM2.5 are complex [31] and are generated during the diffusion process [32]. How to quantify the contribution of energy systems to the generation of secondary PM2.5? How to deal with the diffusion effect? Need to be considered. (2) The conversion model of primary pollutants to secondary PM2.5 is not easy to integrate into the system dispatch model. One important reason is that there are nonlinear items in the correlation model [33]. (3) The diffusion of primary PM2.5 and secondary PM2.5 precursors is affected by wind uncertainty, while the generation of secondary PM2.5 is affected by illumination uncertainty [34]. This paper attempts to solve these problems on the basis of reasonable simplification, and establishes the secondary PM2.5 generation and diffusion calculation model suitable for UIHPS system dispatch.

Based on the above analysis, this paper proposes a SEED model for UIHPS considering IDR, taking into account the hazard of secondary PM2.5 caused by system initial emissions. A linearized secondary PM2.5 generation and diffusion model are established and incorporated into environmental-economic costs. The price-based IDR mechanism is modeled as a Stackelberg game, and the backward induction method is used to prove and obtain the Nash equilibrium solution, which is integrated as a constraint set into the SEED. In the case of intelligent environment sensing that provides partial human settlements and background pollutant data, the validity of the proposed model is verified in a virtual city case based on IEEE39 node power grid and 26-node heat network.

The rest of the paper is organized as follows: Section II introduces the problem framework. Section III establishes the GLC calculation methods of PM2.5 considering the secondary PM2.5 generation. Section IV establishes the UIHPS model based on the Stackelberg game-based IDR mechanism, which uses the backward induction method to transform the Nash equilibrium solution into a constraint set. Section V establishes the SEED model based on the above work. Section V conducts case studies and sensitivity analysis. Section VI provides conclusions. Finally, some basic models and study data are presented in the appendix.

II. THE MODEL FRAMEWORK

A. SYSTEM STRUCTURE

The UIHPS model described in this paper is shown in Fig. 1, which consists of TPP, CHP plants, photovoltaic power plants and wind power plants, electric energy transmission networks and integrated energy users in cities. According to the market relationship, it can be divided into two major stakeholders: independent system operator (ISO) and independent energy retailer (IER), as shown in Fig. 1. Among them: ISO is responsible for managing the energy production side and transmission side of UIHPS. ISO earns revenue by selling energy to IER, and also needs to bear the city's energy production and human settlement pollution cost caused by the primary and secondary PM2.5 emissions during the energy production process. The IER is responsible for managing the user aggregation clusters in UIHPS, which have both thermal and electrical energy requirements, and there is a

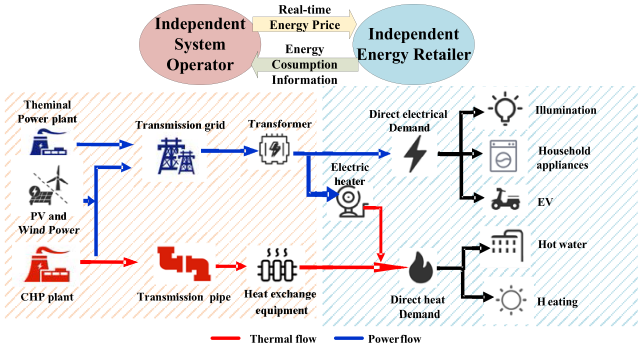

FIGURE 1. UIHPS structure and operation mechanism.

coupling relationship between heat and power loads. Through energy conversion equipment installed in the community or terminal, IER can manage aggregated users to achieve energy demand through different forms of electric/thermal energy load without changing the user's life behavior.

In UIHPS's market trading mechanism, ISO provides a virtual real-time energy price (RTEP)-led transaction to the IER to enhance its overall benefits. IER adjusts according to the RTEP and user cluster energy requirements and preferences provided by ISO, and feeds back IDR load response information (energy consumption information) in this area to reduce its overall cost. After repeating this process, when the interests of the two subjects are mutually constrained to reach equilibrium, the RTEP system and the user's electric heating load guided by the IDR mechanism are determined. The Nash-Stackelberg game (NSG) provides a natural framework to simulate UIHPS's IDR trading mechanism, where ISO is the leader and IER is the follower.

B. MODEL DESCRIPTION

The diffusion of primary PM2.5 and secondary PM2.5 precursors emitted by the unit is affected by wind uncertainty, while the generation of secondary PM2.5 is affected by illumination uncertainty [33], [34]. The uncertainty of light and wind also directly brings uncertainty to the output of new energy units. In order to deal with the uncertainty while considering the primary and secondary PM2.5 hazards, the dispatch problem of UIHPS considering IDR was formulated as a stochastic environmental economic dispatch (SEED) model [35], [36].

1) OBJECTIVE FUNCTION

The objective function of SEED is the system social utility function considering environmental economic profit (also the utility function of ISO). The two parts of PM2.5 comprehensive hazard cost and economic benefit of ISO should be considered in this paper, whose basic form is shown in the first line of (1). The proposed consideration of both the primary and secondary PM2.5 hazards will be analyzed in Sections II.C and III.

2) CONSTRAINTS

This paper considers that (a) sets of constraints that reflect the impact of IDR on the environmental economic profit of the system, (b) PM2.5 total emissions constraints that take into account national standards and regional carrying capacity, (c) conventional systems operation constraints (including network constraints, device constraints, etc.), whose basic form of the constraints is expressed in (1). The (a) group constraints represent the constraint set derived from the backward induction method representing the NSG to obtain an equilibrium solution, whose existence and derivation method will be analyzed in Section II.D and Section III.

$$
\begin{aligned}
obj\ Max.F &= -F^{AP} + F^{PF} \\
&= -(F^{PPM} + F^{SPM} + F^{S}) \\
&\quad + (F^{B} - F^{P} - F^{on}) \\
s.t. &\begin{cases}
\text{(a) IDR constraints:} \\
d = \arg\min\limits_{d \in \Omega_d} c^{IER} \\
\qquad \Downarrow \\
\boldsymbol{C}pr \le \boldsymbol{h} \\
\psi d \le \boldsymbol{g} - \boldsymbol{R}pr \\
\text{(b) PM2.5 total emission constraint:} \\
\varepsilon \le \boldsymbol{EC} \\
\text{(c) System operation constraints:} \\
\boldsymbol{A}\chi \le \boldsymbol{b} \\
\boldsymbol{W}\gamma \le \boldsymbol{m} - \boldsymbol{T}_{\boldsymbol{w}}\chi
\end{cases}
\end{aligned}
\tag{1}
$$

where F^{PPM} is human settlement pollution cost of primary PM2.5, F^{SPM} is human settlement pollution cost of secondary PM2.5, F^{S} is new energy maintenance cost, F^{B} is ISO energy sales revenue, F^{P} is the energy supply cost of the unit and F^{on} is the start-stop cost of the unit. pr represents the decision variables of ISO in IDR, d is the decision variables of IER, ε represents the decision variables of total emission, χ and γ are the decision variables of unit operation in the first and second stages respectively, $\boldsymbol{A}, \boldsymbol{b}, \boldsymbol{W}, \boldsymbol{m}, \boldsymbol{T_w}, \boldsymbol{y}, \boldsymbol{C}, \boldsymbol{h}, \boldsymbol{g}, \boldsymbol{R}$ are the coefficient or parameter matrices.

C. CONTRIBUTION1: CONSIDERING THE COMPREHENSIVE HAZARD OF PM2.5 IN THE OBJECTIVE FUNCTION

The main contribution of this paper is that the proposed SEED model fully considers the PM2.5 comprehensive hazard caused by unit emissions, especially the hazard of the secondary PM2.5. Specifically, the proposed SEED model considers the hazards caused by the following three aspects in the objective function.

1) THE GROUND LEVEL CONCENTRATION OF SECONDARY PM2.5 (SPMGLC)

The toxicity damage degree of secondary PM2.5 to residents' health is mainly determined by SPMGLC, which refers to the amount of GLC contribution caused by secondary PM2.5 generated by complex reactions of NOx, SO_2 (emission of the units) with other background pollutants in the process of diffusion.The main component of the secondary PM2.5 is divided into secondary inorganic aerosol SIA

(which is mainly composed of inorganic components such as sulfate, nitrate and ammonium salts) and secondary organic aerosol (SOA), (mainly refers to PM2.5 organics formed by various chemical reactions in the atmosphere [31]).

The process of converting primary pollutants into secondary PM2.5 is distributed. The generation and diffusion distribution of secondary PM2.5 in this process need to be considered on the basis of the diffusion of NOx and SO_2 precursors discharged from the units. Existing studies typically establish a GLC calculation for primary pollutants as a linear function of the TSD coefficient and the primary pollutant emissions of the units.

$$\Delta GLC_{ikf} \propto \sum_{\tau} G_{i\tau kf} \cdot e_{i\tau} \tag{2}$$

As shown in (2), G_{itkf} is a coefficient that characterizes the GLC contribution of pollutants discharged by unit i at the emission time τ to the regional center f (coordinate (x_f, y_f)) during the observation period k, ΔGLC_{ikf} is the contribution of the pollutants discharged by the unit i throughout the day to the GLC increment of the regional center f during the observation period k, and $e_{i\tau}$ is the primary pollutant emission value of the unit i at the discharge time τ.

On this basis, the linearization calculation function of SPMGLC that can be included in SEED is proposed in Section IV.A.

2) THE GROUND LEVEL CONCENTRATION OF PRIMARY PM2.5 (PPMGLC)

The degree of primary PM2.5's damage to residents' health is mainly determined by PPMGLC, which refers to the amount of GLC contribution caused only by the primary PM2.5 generation and diffusion of the units. Some existing studies [30]–[34] have carried out research on PPMGLC and incorporated it into the objective function of dispatch, in which PPMGLC is usually modeled as a linear function of the TSD coefficients $G_{i\tau kf}$ and the PM2.5 emissions of the units.

For the PM2.5 hazard caused by A and B in this section, based on the calculation of PPMGLC and SPMGLC, and considering the difference between the two to the residents, the harm of PM2.5 to human health is modeled as urban human settlement pollution cost, which is a linear function of PPMGLC, SPMGLC, number of urban areas and the number of regional residents, is included in the objective function. And the PMGLC in this paper, which means the ground level concentration of PM2.5, is the summation of SPMGLC and PPMGLC. The detailed calculation method is shown in Section IV.

3) NEW ENERGY EQUIPMENT MAINTENANCE COSTS UNDER THE INFLUENCE OF PM2.5

In the severe smog environment, the normal operation of photovoltaics and fans requires additional maintenance costs to perform maintenance work such as cleaning photovoltaic panels and fan blades, which is borne by ISO. This paper models the maintenance cost of new energy units as a function related to new energy consumption and atmospheric background pollution levels, and is included in the objective function.

At the same time, in addition to considering the direct harm caused by PM2.5 to residents' health and equipment maintenance, it is also necessary to consider the total amount of PM2.5 emissions from the units from the perspective of regional environmental capacity constraints and government-set emission limits. This effect of PM2.5 is considered as a security constraint rather than an objective function, as shown by constraint group (b) in (1).

D. CONTRIBUTION 2: INCORPORATE AN EQUILIBRIUM CONSTRAINT SET CHARACTERIZING THE IDR IN THE CONSTRAINT

In UIHPS, the optimal result of the NSG game is embodied in the form of Nash equilibrium. The leader, ISO, and the follower, IER, make independent decisions based on their own utility functions, and reasonably pursue the maximization of their own utility. First, the leader ISO develops an energy pricing strategy. Second, the follower IER adjusts the actual energy demand by aggregating the various loads to make the best response load at each time. Next, the ISO adjusts the energy price based on the user's energy needs. It should be pointed out that the system looks for the Nash equalization of the IDR in the solution process of the model, and completes the actual transaction according to the Nash equilibrium result in the actual dispatch process. When the Nash equilibrium is reached, any unilateral policy change of the two entities cannot lead to an increase in its own utility.

In order to easily integrate the NSG search Nash equilibrium process into the SEED model, we try to use the backward induction method to directly derive the Nash equilibrium result into the linear constraint of SEED, and prove the effectiveness of this process in Section IV. The linearization of the system model provides conditions for the effective use of the backward induction method.

Since the ISO has the dispatch right and the information advantage in the UIHPS system, it is necessary to protect the user-side rights through the following restrictions on the information interaction mechanism, which avoid the malicious profit of the ISO through the competitive advantage: (1) In the interaction process, the two entities must and only need to share dispatch information related to the interests of both parties, without sharing other information. RTEP is required for ISO, and thermoelectric load information is required for IER. Although the ISO can fit complete information about the IER utility function, such as user preferences, based on the thermoelectric load information in multiple rounds of interaction, it cannot derive privacy data such as internal device composition, power flow process, and life behavior. (2) After the Nash equilibrium is achieved through the virtual complete information dynamic game, the dispatch scheme can be effective only when both parties agree, and converted into actual energy transactions, to ensure that the

actual energy transaction is based on the results of the Nash equilibrium. Under the NSG framework, the ISO and IER utility functions and strategy set models will be established in Section IV.

E. UNCERTAINTY PROCESSING

The day-ahead weather forecast may have large errors, which will lead to the inconvenience of the new energy unit output and the calculation of PPMGLC and SPMGLC in the day-ahead dispatch. It is necessary to use stochastic dispatch to model the proposed problem. Scenario generation methods based on probability distribution functions and predictive data are used to reasonably describe uncertainty. At the same time, this paper assumes that the load forecasting is accurate. The users under the IER management respond completely according to the NSG equilibrium solution, that is, the user side uncertainty is ignored.

This paper assumes that the predicted wind speed and illumination follow the Weibull and Beta distributions respectively, using Monte Carlo simulation to generate their multiple stochastic scenarios based on their probability density functions.

Then, the scenario reduction method introduced in [37]–[39] is used to obtain a typical scenario that is close to the original model to improve the computational efficiency.

In a typical scenario, the photovoltaic power output corresponding to the light intensity can be generated according to (3) [40]. Among them, $P_{pv,STC}$ is the maximum photovoltaic output of PV modules under standard environment (illumination 1000 W/m2, temperature 25°C), T_{pvop} is the converted photovoltaic operating temperature, CPV is the thermoelectric conversion coefficient, and N_{PVM} is the number of photovoltaic modules. Wind power output corresponding to wind speed can be generated according to (4) [41]. Among them, P_w^R is the rated power of the unit. Where P_w^R is the rated power of the unit, ws_w^R is the rated wind speed of the unit, ws_w^{in} is the start-up wind speed of the unit, and ws_w^{out} is the cut-out wind speed of the unit.In addition to the wind and solar data, other background environment data required in SEED is provided by the smart environmental sensing [42], [43].

$$P_{k,pv} = N_{PVM}\left(P_{pv,STC}\frac{BP_k^R}{1000}(1 - CPV(T_{pvop} - 25))\right) \quad (3)$$

$$P_{kw} = \frac{P_w^R}{1 + e^{2CW(WS_{ip} - WS_k)/P_w^{ip}}} \quad (4)$$

III. THE GLC CALCULATION OF PM2.5 CONSIDERING THE SECONDARY PM2.5 GENERATION

The conversion of the secondary PM2.5 involves the interaction of multiple pollutants emitted by the units, the coupling relationship of various processes, involving multiple chemical processes, and the different reaction mechanisms during the day and night, which are mainly carried out during the diffusion of pollutants [32]. the precursors of the reaction include both primary pollutants (including SO2and NOx) emitted by UIHPS energy production, as well as atmospheric background pollutants (including NOx, O3, NH3, etc.) emitted by other sources. Some of the reactions are still in a state of dynamic equilibrium, and the reactants cannot be completely converted.

It can be considered that the process of converting primary pollutants into secondary PM2.5 is distributed, and it is necessary to consider the generation and distribution of secondary PM2.5 in this process on the basis of primary pollutant diffusion, instead of considering the generation of the secondary PM2.5 in a centralized manner first and calculating TSD then. At the same time, this paper focuses on the contribution of power and thermal production to secondary PM2.5 in UIHPS, ignoring the secondary PM2.5 concentrations caused only by background contaminants.

In order to consider the generation and diffusion of the secondary PM2.5 in the SEED model of UIHPS, this paper first makes some reasonable simplifying hypotheses, and proposes a simplified model of secondary PM2.5 transformation for SEED, which establishes a SPMGLC function that integrates the secondary PM2.5 hazard into SEED.

A. SIMPLIFIED ASSUMPTIONS

a. Since the TSD coefficient of the primary pollutant and the secondary PM2.5 in the diffusion process are basically the same, only the attenuation coefficient different, this paper assumes that the PMGLC increment generated by the secondary PM2.5 produced by primary pollutants in the diffusion at a certain moment in a certain place is equivalent to the one after the primary pollutants diffuse to this location at this time.

b. Assume that the conversion ratio of the reactants in the dynamic equilibrium chemical reaction is a constant during the day or night of the same natural day.

c.Assume that in SPMGLC, the contributions of SIA and SOA are almost equal. Studies have shown [31], [32] that SIA and SOA have similar contributions to PM2.5 concentrations in air pollution. Since the generation mechanism of SOA is very complicated and its GLC is difficult to calculate, this paper makes this hypothesis to numerically simulate the contribution of SOA based on the calculation results of SIA.

d. For SIA, this paper only considers the formation of sulfate and nitrate paper, and ignores the interaction between the reaction rate and the conversion ratio between the chemical reactions that produce sulfate and nitrate.

Through the above reasonable hypothesis, the primary PM2.5 diffusion model and the linearized PM2.5 transformation model can be integrated to simulate the distributed generation and diffusion of the secondary PM2.5, and calculate the contribution to SPMGLC of the pollutant emissions from power and heat production. The following is a description of the primary pollutant spatiotemporal diffusion model and the secondary PM2.5 transformation model used in this paper, and a discussion of their integration methods.

B. CONVERSION MODEL OF PRIMARY POLLUTANTS TO SIA

The formation process of SIA in the secondary PM2.5 is shown in Fig. 2, which mainly includes the chemical process of converting SO_2 to SO_4^{2-}, and the one of converting NO_x to NO_3^-. The former contains the gas phase reaction process and the liquid phase reaction process, which is directly affected by sunlight and atmospheric humidity, and is a mainly one-way chemical reaction; the latter is mainly a gas phase reaction process, which is carried out in two stages, wherein the first stage is a one-way reaction and the second stage is a dynamic equilibrium reaction process. Both types of chemical reactions are affected by atmospheric oxidants represented by O_3. In this paper, the background concentration of O_3 is used to indicate the degree of oxidation of the precursor to the atmosphere, and the light intensity and relative humidity are used to express the influence of solar illumination and atmospheric humidity on the reaction rate [34], using the background precursor concentration and the plume concentration of the precursor distinguishes the influence of background pollutants and unit emission pollutants, and establishes a daytime SIA conversion rate model. The conversion principles of SO_2 and NO_x during the nighttime are different from those during the day, and the reaction rate during the nighttime is much lower than that during the day, set to 0.2% and 2.0% respectively.

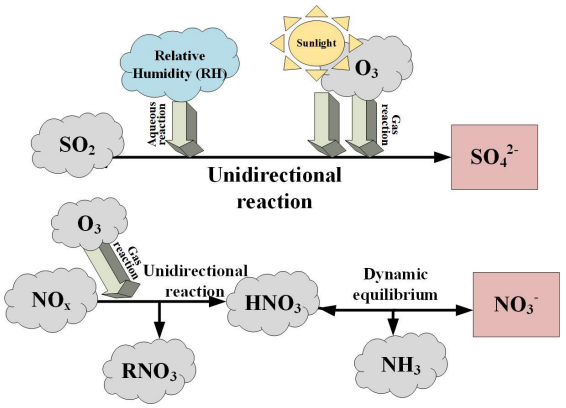

FIGURE 2. Conversion process of primary pollutants to SIA.

Then the hourly GLC conversion calculations of SO_2 and NO_x to SO_4^{2-} and NO_3^- can be established as:

$$GLC^{SO_4^{2-}} = \begin{cases} [0.36(BP^R)^{0.55}(BP^{O_3})^{0.71}\varpi^{-1.29} + \\ 3\times10^{-8}(BP^{RH})^4]\cdot(ep^{SO_2}+BP^{SO_2}) & BP^R>0 \\ 0.2\%\cdot(ep^{SO_2}+BP^{SO_2}) & BP^R=0 \end{cases} \quad (5)$$

$$GLC^{NO_3^-} = \begin{cases} [12.61\cdot(BP^{O_3})^{1.45}\varpi^{-1.34}(ep^{NO_x})^{-0.12}]\cdot \\ (ep^{NO_x}+BP^{NO_x})\cdot tr_{HNO_3} & BP^R>0 \\ 2\%\cdot(ep^{NO_x}+BP^{NO_x})\cdot tr_{HNO_3} & BP^R=0 \end{cases} \quad (6)$$

where $GLC^{SO_4^{2-}}$ is the GLC increment of SO_4^{2-} in secondary PM2.5 caused by SO_2 emission, $GLC^{NO_3^-}$ is the GLC increment of NO_3^- in secondary PM2.5 caused by NO_x emission, ep^{SO_2} is the SO_2 plume concentration caused by emission, ep^{NO_x} is the NO_x plume concentration caused by emission, ϖ is atmospheric stability, BP^R is the intensity of light, BP^{SO_2} is the concentration of background SO_2, BP^{NO_x} is the concentration of background NO_x, BP^{O_3} is the concentration of background ozone, BP_{RH} is the relative humidity of the atmosphere, tr_{HNO_3} is the dynamic equilibrium constant of the second stage reaction of the transformation from NO_x to NO_3^-. Combined with Simplified assumptions 2, this paper takes $tr_{HNO_3}=0.3$ according to the actual statistical data of a city in northern China.

In the initial formula, equation (6) is nonlinear. Linearization must be done to incorporate the dispatch model for the following three reasons:

(1) As far as the whole society is concerned, the source of precursors generated by the secondary PM2.5 is complex, not only from the energy system, but also from other industries such as industry, transportation, etc, and is also affected by background pollutants. The non-linear SPMGLC calculations cannot be linearly superimposed, which will make it difficult to separately analyze the contribution of primary pollutants emitted by UIHPS to SPMGLC, while ignoring the effects of only background pollutants and other industrial pollutants.

(2) As far as UIHPS is concerned, its contribution to SPMGLC is also composed of the contributions of various TPP and CHP units. The contribution of different units to SPMGLC will become an important basis for differentiated scheduling. Because the nonlinear model cannot be linearly superimposed, it is difficult to distinguish the contribution degree of different units, which brings obstacles to the integration of SPMGLC model and scheduling model.

(3) After the SPMGLC function is integrated into the objective function of the system, the nonlinearity will affect the validity of the NSG equilibrium solution constraint set proved and derived by the backward induction method.

Set the coefficient $tr_{NO_3} = 12.61\cdot(BP^{O_3})^{1.45}\varpi^{-1.34}tr_{HNO_3}$. Then when $BP^R>0$, (5) can be expressed as:

$$\begin{aligned}\Delta GLC_{ifk}^{NO_3^-} &= tr_{NO_3}(ep^{NO_x})^{-0.12}(ep^{NO_x}+BP^{NO_x}) \\ &= tr_{NO_3}\cdot(ep^{NO_x})^{0.88}+BP^{NO_x}\cdot(ep^{NO_x})^{-0.12}\end{aligned} \quad (7)$$

Taylor expansion is performed on (7) near $ep^{NO_x} = 0.35BP^{NO_x}$, where the higher-order terms above three are ignored, and the quadratic function approximation relation of $\Delta em_{day}^{NO_3}$ about ep^{NO_x} is obtained as:

$$\begin{aligned}&GLC^{NO_3^-}(ep^{NO_x}) \\ &= 1.368tr_{NO_3}\cdot(BP^{NO_x})^{0.88} \\ &\quad + 0.295tr_{NO_3}\cdot(BP^{NO_x})^{-0.12}\cdot ep^{NO_x} \\ &\quad + 0.451tr_{NO_3}\cdot(BP^{NO_x})^{-1.12}\cdot(ep^{NO_x})^2\end{aligned} \quad (8)$$

In order to verify the accuracy of the approximation of (8) to (7), a quadratic function fit is established as shown

in Fig. 3. When ϖ, BP^{NO_x}, BP^{O_3} is set to 6, 100 μg/m^3, 20 μg/m^3 respectively, the deviation caused by the approximate calculation within the rage of 10 to 100 μg/m^3 for variable ep^{NO_x} is shown in Table 1. Results show that (8) has better accuracy and can satisfy the calculation requirements of energy system in the normal operation interval.

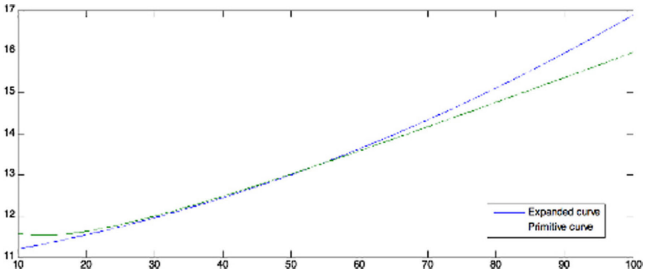

FIGURE 3. Comparison between quadratic function fitting and original function.

TABLE 1. Comparison between quadratic function fitting and original calculation.

NO_x plume concentration (μg/m^3)	20	40	60	80	100
Original result (μg/m^3)	11.63	12.48	13.59	14.77	15.98
Deviation rate (%)	−3.32	−0.29	0.37	2.37	5.70

Referring to the piecewise linearization method for power generation cost in the combined model of the units [44], it is convenient to establish a piecewise linearization model for (8) as shown in (9).

Where $\ell^{NO_3^-}$ is the index for segments, NL_n is the total number of segments, $PL_{\ell^{NO_3^-}}$ is the linear coefficient of segment $\ell^{NO_3^-}$, $ep^{NO_x}_{\ell^{NO_3^-}}$ is the NO_x primary emission of segment $\ell^{NO_3^-}$, $ep^{NO_x}_{\ell^{NO_3^-},\max}$, $ep^{NO_x}_{\ell^{NO_3^-},\min}$ are the upper and lower limits of $ep^{NO_x}_{\ell^{NO_3^-}}$ respectively.

$$\begin{cases} GLC^{NO_3^-}(ep^{NO_x}) = \sum_{l^{NO_3^-}=1}^{L^{NO_3^-}} PL_{l^{NO_3^-}} \cdot ep^{NO_x}_{l^{NO_3^-}} \\ +1.368 tr_{NO_3} \cdot (BP^{NO_x})^{0.88} \\ ep^{NO_x}_{l^{NO_3^-},\min} \le ep^{NO_x}_{l^{NO_3^-}} \le ep^{NO_x}_{l^{NO_3^-},\max} \\ ep^{NO_x} = \sum_{l^{NO_3^-}=1}^{L^{NO_3^-}} ep^{NO_x}_{l^{NO_3^-}} + ep^{NO_x}_{\min} \cdot v \end{cases} \tag{9}$$

C. PMGLC MODEL CONSIDERING SECONDARY PM2.5 GENERATION AND DIFFUSION

Since this paper only considers the primary and secondary PMGLC increments caused by primary pollutant emissions from TPP and CHP in UIHPS, the effect of SPMGLC increments associated only with background pollutant concentrations needs to be ignored. At the same time, it is also necessary to consider the influence of the uncertainty of natural conditions such as illumination intensity on the calculation of SPMGLC. Therefore, the constant term unrelated to the unit emission in (5), (9) is removed, and the influence of the stochastic scenario s is considered, respectively:

$$\Delta GLC^{SO_4^{2-}}_{sifk} = \begin{cases} [0.36(BP^R_{sk})^{0.55}(BP^{O_3}_{sk})^{0.71}\varpi^{-1.29}_{sk} \\ +3\times10^{-8}(BP^{RH}_{sk})^4] \cdot ep^{SO_2}_{sifk} & BP^R_{sk} > 0 \\ 0.2\% \cdot ep^{SO_2}_{sifk} & BP^R_{sk} = 0 \end{cases} \tag{10}$$

$$\Delta GLC^{NO_3^-}_{sifk} = \begin{cases} \sum_{l^{NO_3^-}}^{NL_n} PL_{ifk\ell^{NO_3^-}} \cdot ep^{NO_x}_{sifk\ell^{NO_3^-}} & BP^R_{sk} > 0 \\ 2\% \cdot ep^{NO_x}_{sifk} \cdot tr_{HNO_3} & BP^R_{sk} = 0 \end{cases}$$

$$0 \le ep^{NO_x}_{sifk\ell^{NO_3^-}} \le ep^{NO_x}_{ifk\ell^{NO_3^-},\max}$$

$$ep^{NO_x}_{sifk} = \sum_{\ell^{NO_3^-}}^{NL_n} ep^{NO_x}_{sifk\ell^{NO_3^-}} + ep^{NO_x}_{ifk,\min} \cdot v_{sik} \tag{11}$$

where k is the index for time periods, s is the index for scenarios, i is the index for TPP, f is the index for monitoring areas, $\Delta GLC^{SO_4^{2-}}_{sifk}$ and $\Delta GLC^{NO_3^-}_{sifk}$ are the GLC increment of SO_4^{2-} in SPMGLC caused by SO_2 emission and that of NO_3^- in SPMGLC caused by NO_x emission only of unit i in a period of time k for monitoring area f in scenario s respectively.

Simultaneously, the generation and distribution of the secondary PM2.5 needs to be calculated on the basis of the diffusion of primary pollutant. By hypothesis a, the plume concentration of the SO_2 and NO_X precursor pollutants puff emitted by the unit spreads to the ground level is the concentration of the precursor plume generated by the SIA in (10) and (11). $ep^{NO_x}_{sifk}$, $ep^{SO_2}_{sifk}$ calculated by:

$$\begin{cases} ep^{NO_x}_{sifk} = \frac{1}{N_{puff}} \cdot \sum_{\tau=t_{k_\tau-1}}^{t_{k_\tau}-\Delta t_p} \exp[-\frac{t_k-\tau}{T^{NO_x}_{res}}] \cdot G_{i\tau kf} \cdot e^{NO_x}_{sik_\tau} \\ ep^{SO_2}_{sifk} = \frac{1}{N_{puff}} \cdot \sum_{\tau=t_{k_\tau-1}}^{t_{k_\tau}-\Delta t_p} \exp[-\frac{t_k-\tau}{T^{SO_2}_{res}}] \cdot G_{i\tau kf} \cdot e^{SO_2}_{sik_\tau} \end{cases} \tag{12}$$

where τ is the index for emission time, k_τ is the period where τ is located, Δk is the unit dispatch time, N_{puff} is the amount of smoke mass emitted by a unit during the unit scheduling time, T_{res} is the residence time of pollutants.

PPMGLC discharged by the unit is calculated by:

$$\begin{aligned} \Delta PM^{PG}_{sifk} &= ep^{pm2.5}_{sifk} \\ &= \frac{1}{N_{puff}} \cdot \sum\nolimits_{\tau=t_{k_\tau-1}}^{t_{k_\tau}-\Delta t_p} \exp[-\frac{t_k-\tau}{T^{pm2.5}_{res}}] \\ &\quad \cdot G_{i\tau kf} \cdot e^{pm2.5}_{sik_\tau} \end{aligned} \tag{13}$$

The calculation method of $G_{i\tau kf}$ considering the influence of the atmospheric boundary layer is described in [29].

The primary pollutant emissions of the TPP $e_{ik_\tau}^{NO_x}$, $e_{ik_\tau}^{SO_2}$ and $e_{ik_\tau}^{pm2.5}$ are modeled as a quadratic function of the unit's output and linearized in phases, while the primary pollutant emissions of the CHP units are modeled using the corner method described in Appendix (A9)–(A12). The calculation formula for linearized unit emissions considering the unit's pollutant control measures is as shown in (A13)–(A16).

Bringing (12) into (10) and (11) can obtain the GLC of the ions in the SIA: $\Delta GLC_{sifk}^{SO_4^{2-}}$ and $\Delta GLC_{sifk}^{SO_4^{2-}}$, according to the ion concentration's mass conversion relationship with the sulfate and the nitrate, respectively. By the hypothesis b, the SPMGLC of SIA is calculated by:

$$\Delta PM_{sifk}^{SIA} = 1.375\Delta GLC_{sifk}^{SO_4^{2-}} + 1.28\Delta GLC_{sifk}^{NO_3^-} \tag{14}$$

By hypothesis c, ΔPM_{sifk}^{SG} is obtained represented by (15), which is the calculation formula of SPMGLC increment caused by unit i in the monitoring area f at time k and scenario s.

$$\begin{cases} \Delta PM_{sifk}^{SIA} = \Delta PM_{sifk}^{SOA} \\ \Delta PM_{sifk}^{SG} = \Delta PM_{sifk}^{SOA} + \Delta PM_{sifk}^{SIA} \end{cases} \tag{15}$$

where ΔPM_{sifk}^{SOA} is the GLC increment of SOA.

The calculation equation for the increment of PMGLC and SPMGLC of CHP is identical to that of thermal power units except that index is changed from i to j.

Supported by the background pollutant data of smart environmental sensing [45], [46], the SPMGLC and PPMGLC calculation functions constructed in this section will incorporate the human health effects of PM2.5 into the objective function of SEED in Section IV.

IV. UIHPS MODEL BASED ON NSG

A. UTILITY FUNCTION OF ISO (LEADER) UNDER NSG

The utility function of ISO (leader), as described in (2), consists of the cost of human settlement pollution cost F^{PM} generated by PPMGLC and SPMGLC, equipment maintenance cost F^S, and unit start-stop cost F^{on}, unit operating cost F^P, and ISO sales revenue F^B. Among them, F^{on}, F^P, F^B constitute the actual economic profit of ISO F^{PF}, which can be expressed as:

$$F^{PF} = -F^{on} + F^B - (F^P + F^S) \tag{16}$$

It should be pointed out that the actual economic profit of ISO as shown in (16). Human settlement pollution costs generated by PPMGLC and SPMGLC not only can be used as the actual taxes collected by the government to compensate for the health hazards caused by ISO emissions, but also can be included as a virtual cost into the dispatch model to assess the effectiveness and economic costs of mitigating ISO emissions hazards through dispatch.

1) Start-up cost of units is calculated by:

$$F^{on} = \sum_k^K \sum_i^I \pi_{ik}^{on}\omega_{ik}^{on} + \sum_k^K \sum_j^J \pi_{jk}^{on}\omega_{jk}^{on} \tag{17}$$

K is the total number of dispatching period, I is the total number of thermal power units, J is the total number of CHP units.

2) Operating costs of units can be described as:

$$F^P = \sum_k^K \sum_i^I c_{ki}^P + \sum_k^K \sum_j^J c_{kj}^{CHP} \tag{18}$$

where the power generation cost of coal-fired units is generally modeled as a quadratic function of power.

The joint linearization method of the coal-fired units' power generation costs and primary pollutant emission model is shown in Appendix A. The linearized model represented by (19)–(20) is obtained by:

$$c_{ik}^P = A_i^P v_{ik} + \sum_{\ell^p}^{NL_i} PL_{ik\ell^p}^P \delta_{ik\ell^p}^P \tag{19}$$

$$p_{ik} = \sum_{\ell^p}^{NL_i} \delta_{ik\ell^p}^P + \underline{p_i} v_{ik} \quad 0 \le \delta_{ik\ell^p}^P \le \delta_{i\ell^p,\max}^P \tag{20}$$

where v_k is a binary variable indicating the running status of the unit, which takes 1 if started up, 0 otherwise. ℓ^p is a linear segmented index, NL_i is the number of segments, A_i^P and $PL_{ik\ell^p}^P$ is the linearization coefficient, and $\delta_{ik\ell^p}^P$ is the linearization variable.

$$c_{kj}^{CHP} = v_{kj} \sum_m^{NL_m} \alpha_{kj}^m C_{jm}^{CHP} \tag{21}$$

$$\begin{cases} p_{jk} = \sum_m^{NL_m} \alpha_{jkm}^m P_{jm}^m \\ q_{jk} = \sum_m^{NL_m} \alpha_{jk}^m Q_{jm}^m \\ 0 \le \alpha_{jkm}^m \le 1 \\ \sum_m^{NL_m} \alpha_{jkm}^m = 1 \end{cases} \tag{22}$$

For the CHP units decoupled from the electric output and the thermal output, a linear superposition of the angular point operation data as shown in Fig. 4 is often used to indicate the operating space boundary of the units [23].

The operating cost of units based on the corner point model is expressed as (21)–(22), Where m is the index for the corner point, NL_m is the total number of corner points, p_{jk} is the unit's electric output, q_{jk} is the unit's thermal output, α_{kj}^m is the running coefficient of the corner point m, C_{jm}^{CHP} is the running cost of the corner point m, and P_{jm}^m is the electric output of the corner point m, Q_{jm}^m is the heat output of the corner point m.

3) Revenue from energy sales

Revenue from energy sales is the energy income that ISO participates in NSG, when it reaches Nash equilibrium (NE), according to its own quotation and energy purchases from

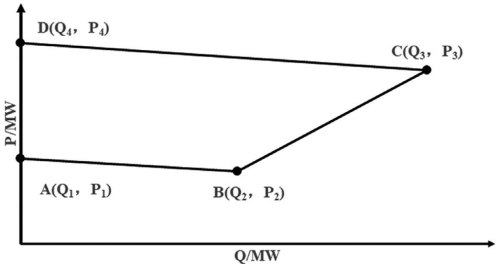

FIGURE 4. CHP unit Schematic diagram of the corner model.

IER feedback, which is paid by IER as:

$$F^B = \sum_{k}^{K}\sum_{u}^{U} F^B_{ku} = \sum_{k}^{K}\sum_{u}^{U}(B^e_{ku}pr^e_{ku} + B^h_{ku}pr^h_k) \quad (23)$$

where u is the index for the user participating in IDR, U is the number of users, pr^e_{ku} is the real-time electricity price issued by ISO, pr^h_k is the real-time heat price issued by ISO, B^e_{ku} is the electric load of user response, and B^h_{ku} is the heat load of user response.

It should be pointed out that in addition to the actual economic profit shown in (16), the comprehensive environmental costs generated by PPMGLC and SPMGLC $F^{AP} = F^{PM} + F^S$ can be used as the actual taxes collected by the government to compensate for the socio-economic losses (such as public medical expenses) caused by the health hazards of residents and equipment caused by ISO emissions, which can also be included as a virtual cost into the dispatch model to assess the effectiveness and cost-effectiveness of mitigating PM2.5 integrated hazards through SEED.

4) Urban average human settlement pollution costs

As mentioned earlier, the hazard level of PM2.5 for residents is determined by GLC, which is affected by PPMGLC and SPMGLC. The SOA in the secondary PM2.5 is chronically toxic, and primary PM2.5 often adsorbs the harmful metal substances generated in the energy production process [47], [48]. The damage mechanism and the action cycle of these two are different so that the modeling of human health hazards costs needs to be based on the PPMGLC and SPMGLC functions shown in (13) and (15), in which the parameters of human settlement pollution costs can be set differentially.

At the same time, from the perspective of public utilities, every citizen in severe smog weather is poisoned by PM2.5 near the ground, and the accumulation of urban population and high concentrations of background pollutants will amplify the total impact of this hazard. That is to say, the greater the population density of a region and the more serious the background pollution, the greater the harm of primary and secondary PM2.5 caused by ISO emissions. Therefore, the utility needs to consider the average pollution hazard of the city based on regional differences.

$$\begin{aligned} F^{PM} &= F^{PPM} + F^{SPM} \\ &= \frac{1}{N_f} PR^{AP}[\sum_{f}^{N_f}\sum_{k}^{K}\sum_{i}^{I} PO_f AP^2_{fk}(\Delta PM^{PG}_{ifk} \\ &\quad + \varsigma \cdot \Delta PM^{SG}_{ifk}) + \sum_{f}^{N_f}\sum_{k}^{K}\sum_{j}^{J} PO_f AP^2_{fk} \\ &\quad \times (\Delta PM^{PG}_{jfk} + \varsigma \cdot \Delta PM^{SG}_{jfk})] \end{aligned} \quad (24)$$

Based on the above analysis, the calculation function of the urban human settlement health cost is established (24), where the values of the air pollution level parameters indicating the background pollution level AP_{fk} are shown in Table 2.

TABLE 2. The parameters of air pollution level.

Background concentration of PM2.5 (μg/m^3)	Air quality level [1]	Air pollution level parameter AP_{fk}
$0 \sim 12$	Excellent	1
$12 \sim 35.4$	Good	2
$35.4 \sim 55.4$	Mildly polluted	3
$55.4 \sim 150.4$	Moderately polluted	4
> 150.4	Severely polluted	5

Where F^{PPM} and F^{SPM} is the contribution of primary PM2.5 and secondary PM2.5 respectively. The value of the air pollution level parameter AP_{fk} which characterizes the background pollution level is shown in Table 2. PO_f is the population of the area f, PR^{AP} is the hourly unit human settlement pollution cost parameter caused by primary PM2.5, and ς is the weight factor of the secondary PM2.5 human health hazard (compared to primary PM2.5).

5) New energy maintenance costs

The maintenance cost of new energy units is modeled as the function (25) related to new energy consumption and air pollution level parameters in this paper.

$$F^S = \sum_{k}^{K}\sum_{w}^{W} AP^2_k p_{kw} PR^{wind}_w + \sum_{k}^{K}\sum_{pv}^{PV} AP^2_k p_{k,pv} PR^{pv}_{pv} \quad (25)$$

where w is the index for the fan, W is the number of fans, p_{kw} is the fan output, PR^{wind}_w is the unit maintenance cost of the fan, pv is the index for the photovoltaic power plant, PV is the number of photovoltaic power plants, $p_{k,pv}$ is the photovoltaic output, and PR^{pv}_{pv} is the maintenance cost of the photovoltaic unit.

B. COST FUNCTION OF IER (FOLLOWER) UNDER NSG

The coupling relationship between the external electric and thermal load of the IER and the electric and heat demand of the IER internal users is shown on the right side of Fig. 1. Among them, the energy demand generated by the user's life behavior is defined as direct energy demand, such as direct electric energy demand generated by household appliances, lighting, electric vehicle charging, etc, and direct thermal

energy demand generated by the behavior of changing room temperature and heating water. The actual load is the energy that the IER purchase from the ISO to meet the direct energy needs of users, while the thermoelectric load is converted by energy conversion devices such as power transformers, electric heating devices, and heat exchange devices to meet the direct energy needs of users. The following equations of energy conversion are constructed for this.

$$\begin{bmatrix} \alpha_{uk}^{e}\beta_{u}^{e} & 0 \\ \alpha_{uk}^{e2h}(t)\beta_{u}^{e2h} & \beta_{u}^{h} \end{bmatrix} \begin{bmatrix} B_{suk}^{e} \\ B_{suk}^{h} \end{bmatrix} = \begin{bmatrix} ED_{uk} \\ HD_{uk} \end{bmatrix} \tag{26}$$

where β_u^e, β_u^{e2h} and β_u^h represent the conversion efficiency of the transformer and the electrothermal conversion device, respectively; α_{uk}^e and α_{uk}^{e2h} respectively represent the direct power supply ratio and the electric heating ratio of the user u's electrical load u during the period k. B_{ku}^e and B_{ku}^h respectively represent the actual power purchase (actual electrical load) and heat purchase (actual heat load) of the user, and ED_{uk} and HD_{uk} respectively represent the direct electric energy demand required by the user's life.

In order to simplify the derivation process, according to the actual operating experience [49], the conversion efficiency of the heat exchange equipment and the transformer is approximately set to 1. According to the (26), the relationship between the thermoelectric load of users can be obtained as:

$$B_{uk}^{h} = -\frac{\beta_k^{e2h}}{\beta_k^h}B_{uk}^{e} + \left(\frac{1}{\beta_k^h}HD_{uk} + \frac{\beta_k^{e2h}}{\beta_k^e\beta_k^h}ED_{uk}\right) \tag{27}$$

According to (27), the thermal load and the electrical load are linear. The thermal load can be characterized by the electrical load, thereby various indicators of the comprehensive demand response can be directly calculated.

By definition, the cost of IER can be divided into two types: purchase cost and preference cost. Assumed that users do not change their life behavior and energy demand when participating in IDR, and the demand response of users is independent of each other and fully responds to the management of energy retailers to be aggregated, the operating cost of the IER c^{IER} is modeled as:

$$c^{IER} = \sum_{k}^{K}\sum_{u}^{U}\left(F_{ku}^{B} + c_{ku}^{pre}\right) \tag{28}$$

1) The cost of purchasing energy c_{uk}^B is the cost of purchasing electricity and heat from IER to ISO. According to the RTEP provided by ISO, it can be modeled as:

$$c_{ku}^{B} = F_{ku}^{B} = B_{ku}^{e}pr_{ku}^{e} + B_{ku}^{h}pr_{k}^{h} \tag{29}$$

2) The cost of preference [50] is defined as the unsatisfactory cost brought by the difference between the actual energy load and the preference energy load of users under the premise of satisfying the user's direct energy demand. Because of the linear coupling relationship between the electric load and the thermal load, the preferred electric load E_{uk}^p is defined, and the quadratic function is used to model the user's deviation of the preference cost as:

$$c_{ku}^{pre} = \frac{\lambda_{uk}}{2E_{uk}^{e}}(B_{ku}^{e})^2 - \lambda_{uk}B_{ku}^{e} + \frac{\lambda_{uk}}{2}(E_{uk}^{e})^2 \tag{30}$$

C. SECURITY CONSTRAINTS

1) BALANCE CONSTRAINTS

Balance constraints of electric power and thermal power [51]–[53].

$$\begin{cases} \sum_{i}^{N_i} p_{ik} + \sum_{j}^{J} p_{jk} + \sum_{w}^{W} p_{wk} + \sum_{pv}^{PV} p_{k,pv} \\ -\sum_{u}^{U} B_{uk}^{e} + \sum_{r^P}^{NL_p} \frac{1}{x_{r^P n^P}}(\theta_{r^P k} - \theta_{n^P k}) = 0 \\ \sum_{j}^{J} q_{jk} - \sum_{u}^{U} B_{uk}^{h} + \sum_{r^H}^{NL_h} \\ (Q_{n^H r^H k} - 2\pi \frac{T_j - T_e}{\sum R_h} L_{n^H r^H}) = 0 \\ -\pi \le \theta_{r^P k}, \theta_{n^P k} \le \pi \\ \theta_{ref,k} = 0 \end{cases} \tag{31}$$

where r^P, n^P is the index for the grid node, NL_p is the number of grid nodes, $\theta_{ref,k}$ is the grid reference power angle, r^H, n^H is the index for the heat network node, NL_h is the number of heat network nodes, and Q_{nrk} is the heat energy transmitted on the pipeline of node $n^H - r^H$, T_j is the outlet hot water temperature of the CHP unit j, T_e is the ambient temperature around the pipeline, R_h is the ambient thermal resistance of the pipeline, and L_{nr} is the length of the pipeline.

2) PM2.5 PRIMARY EMISSION CONSTRAINT

$ET_{\lim}^{pm}$ represents the total amount of PM2.5 discharged by the system during the dispatch period, whose value is set according to the special limit in the national standard [54] issued by the Chinese government.

$$\sum_{i}^{I}\sum_{k_\tau}^{K} e_{ik_\tau}^{pm2.5} + \sum_{j}^{J}\sum_{k_\tau}^{K} e_{jk_\tau}^{pm2.5} \le ET_{\lim}^{pm} \tag{32}$$

3) PRICE CONSTRAINTS OF IDR

$$PR_{\min}^{e} \le pr_{k}^{e} \le PR_{\max}^{e} \tag{33}$$

4) SPACE CONSTRAINT OF IDR

$$\begin{cases} ED_{uk} \le B_{uk}^{e} \le B_{uk,\max}^{e} \\ B_{uk,\min}^{e} \le B_{uk}^{h} \le HD_{uk} \end{cases} \tag{34}$$

5) CONSUMPTION CONSTRAINTS OF NEW ENERGY

$$\begin{cases} 0 \le p_{kw} \le P_{kw}^{\max} \\ 0 \le p_{k,pv} \le P_{k,pv}^{\max} \end{cases} \tag{35}$$

where $P_{kw}^{\max}$, $P_{k,pv}^{\max}$ is the upper and lower limits of the fan and photovoltaic output respectively.

6) OPERATIONAL CONSTRAINTS OF TPP AND CHP UNITS

See Appendix A for equations (A1)–(A5), (A9)–(A16).

D. BALANCED SOLUTION OF NSG

1) NASH-STACKELBERG GAME

In UIHPS, ISO as a leader and IER as followers can analyze the market participants and their income functions through information interaction to establish an IDR trading mechanism modeled by the Stackelberg game. The optimal result of the game is embodied in the form of Nash equilibrium. Under this mechanism, the leader ISO maximizes its benefits based on the IER's optimal response at each time period to make decisions.

First, the leader, ISO, develops an energy pricing strategy. Second, the followers, IER, adjust the actual energy demand by aggregating the various loads to make the best response at each time. Next, the ISO adjusts the energy price based on the user's energy needs, and repeats this process until the energy balance between the energy price and the IDR is achieved. When the Nash equilibrium is reached, any one-sided policy change of the two subjects cannot lead to an increase in its own utility. The Nash equilibrium optimal strategy of this Stackelberg game can be expressed as equation (36).

$$\begin{cases} (pr_k^e, B_{uk}^{e*}) = \arg \max\limits_{\{pr_k^e, B_{uk}^e\}} f_{PEU}(pr_k^e, B_{uk}^{e*}) \\ s.t.\ \ (B_{uk}^{e*}) = \arg \min\limits_{\{B_{uk}^e\}} c_k^{IER}(pr_k^{e*}, B_{uk}^e) \end{cases} \tag{36}$$

2) PROOF AND SOLUTION OF NASH EQUILIBRIUM

According to the existence of the Nash equilibrium of the Stackelberg game [55], there is only one Nash equilibrium solution when the following conditions are met.

a.The strategy set of each player is nonempty, convex, and compact;

b.The cost functions of the followers are continuous convex functions about its own set of strategies;

c.The utility function of the leader is a continuous concave function of its own set of strategies.

For condition a: it can be seen from (19)–(22), (31)–(35), (A1)–(A5), (A9)–(A16) that the feasible operation region constraints of the ISO and IER strategy sets are linear and convex constraints. The feasible operation region sets are feasible, defined as nonempty, convex, and compact;

For condition b: According to 2.2, the NSG established in this paper belongs to the complete information dynamic game. The backward induction method [52] is used to make hypothesis, trying to solve the analytical expression of the IER's optimal response strategy, and then verify the existence and validity of this analytical solution by proving condition b.

Because of different scenarios, users, and time can be linearly superimposed [47], [48], the analysis in this section uses a single scenario and a single load at a single time.

Bring (27) into (29)–(31) as:

$$c_{ku}^{IER} = \frac{\lambda_{uk}}{2E_{uk}^e}(B_{ku}^e)^2 + (pr_k^e - \lambda_{uk} - \frac{\beta_u^{e2h} pr_k^h}{\beta_u^h})B_k^e + [\frac{\lambda_{uk}}{2}(E_{uk}^e)^2 + pr_k^h(\frac{1}{\beta_u^h}HD_{uk} + \frac{\beta_u^{e2h}}{\beta_u^e \beta_u^h}ED_{uk})] \tag{37}$$

The first derivative of its strategy B_{sku}^e is calculated by:

$$\frac{dc_{uk}^{IER}}{dB_{uk}^e} = \frac{\lambda_{ku}}{E_{ku}^e}B_{ku}^e + (pr_k^e - \lambda_{ku} - \frac{\beta_u^{e2h} pr_k^h}{\beta_u^h}) \tag{38}$$

By let $\frac{dc_{ku}^{EUER}}{dB_{ku}^e} = 0$, the analytic function of the best response is expressed as:

$$\frac{d^2 c_{ku}^{IER}}{d(B_{ku}^e)^2} = \frac{\lambda_{ku}}{E_{ku}^e} > 0 \tag{39}$$

Since the value of (40) is always positive, and the strategy set is nonempty, convex, and compact, it can be proved that the cost function of IER is convex for its policy set. The optimal response strategy represented by (39) is optimal and unique, and condition b is proved.

For condition c: For the ISO utility function (16), after linearizing the model according to (9), (19)–(22), (A9)–(A12), (A16), it is easy to obtain F^{AP}, F^{on}, F^P, F^S as linear convex functions. Only the concavity and convexity of F^B is needed to investigate.

(39) is brought into (29) as:

$$F_{ku}^B = c_{ku}^B = -E_{ku}^e(pr_k^e)^2 + (E_{ku}^e + \frac{E_{ku}^e \beta_u^{e2h} pr_k^h}{\beta_u^h \lambda_{ku}})pr_k^e + B_{ku}^h pr_k^h \tag{40}$$

The second derivative of the strategy set pr_k^e in (40) is calculated by:

$$\frac{d^2 F_{ku}^B}{d(pr_k^e)^2} = -2E_{ku}^e < 0 \tag{41}$$

Since the policy set of the ISO is nonempty, convex, and compact, and the value of the (41) is always negative within the range of values, it can be proved that the utility function of the ISO is concave for its policy set pr_k^e. The condition c is proved.

According to the above analysis, it can be proved that the IDRSG described in this paper has one and only one Nash equilibrium solution.

The optimal response strategy obtained by the backward induction method shown in (39) is substituted into (34), (35), and the constraints are updated as:

$$\begin{cases} (1+\frac{\beta_u^{e2h} pr_k^h}{\beta_u^h \lambda_{ku}}) - \frac{B_{k,\max}^e}{E_{ku}^e} \le pr_k^e \le (1 + \frac{\beta_u^{e2h} pr_k^h}{\beta_u^h \lambda_{ku}}) - \frac{ED_{ku}}{E_{ku}^e} \\ (1+\frac{\beta_u^{e2h} pr_k^h}{\beta_u^h \lambda_{ku}}) - PR_{\max}^e \le B_{ku}^e \le (1 + \frac{\beta_u^{e2h} pr_k^h}{\beta_u^h \lambda_{ku}}) - PR_{\min}^e \end{cases} \tag{42}$$

Based on the above analysis, after considering (39) and inequality constraint (42), the process of solving the NSG

equilibrium solution can be transformed into a constraint set and integrated into the optimization problem of the ISO utility function shown in (22). Among them, the equivalent process can be described as: through a small number of iterative interactions, ISO fits the cost parameter of IER and solves its own optimal bidding strategy, and then brings in the cost function of IER to calculate the optimal load response, which can get a balanced solution. This dispatch method based on the backward induction method can avoid repeated interactions between the two parties involved in the game. Compared with the heuristic method, it has the advantages of less iterations, faster calculation speed and easy expansion. It should be emphasized that in the UIHPS system model introducing the secondary PM2.5 calculation function, the linearization of the time-space distribution function of the second PM2.5 as shown in equation (9) and (19)–(22), The linearization of the unit operating cost and emission function shown in (A9)–(A12), (A16) is the only necessary and effective condition for ensuring the NSG equilibrium solution constraint set of the SEED derived by the backward induction method.

V. TWO-STAGE SEED MODEL

Based on the utility functions and constraints of UIHPS described in Section IV, the two-stage original SEED model is established. Among them, the first stage is the dispatch stage, which determines the on/off state of the unit and the predetermined power output, and the second stage is the operation stage, which adjusts the output of the unit according to different scenarios and guides the IER to participate in the IDR to adapt to environmental uncertainty. With a finite number of scenarios $s_1, \ldots, s_{N_s}$ subject to probability masses $\rho_1, \ldots, \rho_{N_s}$, a one-stage deterministic equivalent [56] of the two-stage stochastic problem can be proposed in order to jointly optimizes these two stages, which will determine the appropriate dispatch decision variables and guide the IDR transactions.

$$
\begin{aligned}
obj: \max F
&= \rho_s F_s^B - F^{on} - \sum_s^S \rho_s F_s^P \\
&\quad - \sum_s^S \rho_s (F_s^{PPM} + F_s^{SPM} + F_s^S) \\
&= \sum_s^S \rho_s \sum_k^K \sum_u^U (B_{sku}^e pr_{sku}^e + B_{sku}^h pr_k^h) \\
&\quad - (\sum_k^K \sum_i^I \pi_{ik}^{on} \omega_{ik}^{on} + \sum_k^K \sum_j^J \pi_{jk}^{on} \omega_{jk}^{on}) \\
&\quad - \sum_s^S \rho_s [\sum_k^K \sum_i^I (A_i^P v_{ik} + \sum_{\ell^p}^{NL_i} PL_{ik\ell^p}^P \delta_{sik\ell^p}^P) \\
&\quad + \sum_k^K \sum_j^J v_{kj} \sum_m^{NL_m} \alpha_{skjm}^m C_{jm}^{CHP}] \\
&\quad - \sum_s^S \rho_s \frac{1}{N_f} PR^{AP} [\sum_f^{N_f} \sum_k^K \sum_i^I PO_f AP_{fk}^2 \\
&\quad \times (\Delta PM_{ifk}^{PG} + \varsigma \cdot \Delta PM_{ifk}^{SG}) \\
&\quad + \sum_f^{N_f} \sum_k^K \sum_j^J PO_f AP_{fk}^2 (\Delta PM_{ifk}^{PG} + \varsigma \cdot \Delta PM_{ifk}^{SG})] \\
&\quad - \sum_s^S \rho_s (\sum_k^K \sum_w^W AP_{sk}^2 p_{skw} PR_w^{wind} \\
&\quad + \sum_k^K \sum_{pv}^{PV} AP_{sk}^2 p_{sk,pv} PR_{pv}^{pv})
\end{aligned} \tag{43}
$$

A. OBJECTIVE FUNCTION

According to (2), the objective function of the SEED model is described as (43).

B. CONSTRAINTS

In the first phase, the constraints of the day-ahead dispatch stage include: unit operating constraints (19)–(22), (A1)–(A5), (A9)–(A14), (A16), power balance constraints (31), total emissions constraints (32), IDR constraints (33), (34), (39), (43), new energy consumption constraints (35), and uncertainty parameter value constraints:

$$
\begin{cases} 0 \le p_{kw} \le \max P_{skw}^{\max} \\ 0 \le p_{k,pv} \le \max P_{sk,pv}^{\max} \end{cases} \tag{44}
$$

$$
BP_k^R = \max BP_{sk}^R \tag{45}
$$

$$
G_{ikk_\tau f} = \max G_{sikk_\tau f} \tag{46}
$$

In the second stage, the constraints for simulating the intraday operational stage is included as:

$$
\begin{cases} \sum_i^I p_{sik} + \sum_j^J p_{sjk} + \sum_w^W p_{swk} + \sum_{pv}^{PV} p_{sk,pv} \\ - \sum_u^U B_{suk}^e + \sum_{r^P}^{NL_p} \frac{1}{x_{r^P n^P}} (\theta_{sr^P k} - \theta_{sn^P k}) = 0 \\ \sum_j^J q_{sjk} - \sum_u^U B_{suk}^h \\ + \sum_{r^H}^{NL_h} (Q_{snr^H k} - 2\pi \frac{T_j - T_e}{\sum R_h} L_{nr}) = 0 \\ -\pi \le \theta_{sr^P k}, \theta_{sn^P k} \le \pi \\ \theta_{ref,sk} = 0 \end{cases} \tag{47}
$$

$$
\begin{cases} p_{sik} = \sum_{\ell^p}^{NL_i} \delta_{sik\ell^p}^P + \underline{p_i} v_{ik} \\ 0 \le \delta_{sik\ell^p}^P \le \delta_{si\ell^p,\max}^P \end{cases} \tag{48}
$$

TABLE 3. Case set.

	Dispatch Target		NSG			
	Economic Profit	Total PM2.5 emissions	PPMGLC	SPMGLC	NSG Considered	NSG Not considered
Case 1	√		√	√	√	
Case 2	√		√		√	
Case 3	√	√			√	
Case 4	√				√	
Case 5	√		√	√		√
Case 6	√		√			√

$$\begin{cases} p_{sjk} = \sum_{m}^{NL_m} \alpha_{sjkm}^{m} P_{jm}^{m} \\ q_{sjk} = \sum_{m}^{NL_m} \alpha_{jsk}^{m} Q_{jm}^{m} \\ 0 \le \alpha_{sjkm}^{m} \le 1 \\ \sum_{m}^{NL_m} \alpha_{sjkm}^{m} = 1 \end{cases} \tag{49}$$

$$\begin{cases} e_{sik}^{NOx} - es_{sik}^{NO_x} + M(1 - sign_{sik}) \ge 0 \\ e_{sik}^{NOx} - [(1 - \mu_i^{NOx}) \times es_{sik}^{NO_x}] + Msign_{sik} \ge 0 \end{cases} \tag{50}$$

$$\begin{cases} 0 \le p_{skw} \le P_{skw}^{\max} \\ 0 \le p_{sk,pv} \le P_{sk,pv}^{\max} \end{cases} \tag{51}$$

$$\sum_{s}^{S} \rho_s (\sum_{i}^{I} \sum_{k_\tau}^{K} e_{sik_\tau}^{pm2.5} + \sum_{j}^{J} \sum_{k_\tau}^{K} e_{sjk_\tau}^{pm2.5}) \le ET_{\lim}^{pm2.5} \tag{52}$$

$$PR_{\min}^{e} \le pr_{sk}^{e} \le PR_{\max}^{e} \tag{53}$$

$$\begin{cases} ED_{uk} \le B_{suk}^{e} \le B_{uk,\max}^{e} \\ B_{uk,\min}^{e} \le B_{suk}^{h} \le HD_{uk} \end{cases} \tag{54}$$

$$B_{ku}^{e} = (E_{ku}^{e} + \frac{E_{ku}^{e} \beta_u^{e2h} pr_k^{h}}{\beta_u^{h} \lambda_{ku}}) - E_{ku}^{e} pr_{ku}^{e} \tag{55}$$

$$\begin{cases} (1 + \frac{\beta_u^{e2h} pr_k^{h}}{\beta_u^{h} \lambda_{ku}}) - \frac{B_{k,\max}^{e}}{E_{ku}^{e}} \le pr_{sk}^{e} \le \\ (1 + \frac{\beta_u^{e2h} pr_k^{h}}{\beta_u^{h} \lambda_{ku}}) - \frac{ED_{ku}}{E_{ku}^{e}} \\ (1 + \frac{\beta_u^{e2h} pr_k^{h}}{\beta_u^{h} \lambda_{ku}}) - PR_{\max}^{e} \le B_{sku}^{e} \le \\ (1 + \frac{\beta_u^{e2h} pr_k^{h}}{\beta_u^{h} \lambda_{ku}}) - PR_{\min}^{e} \end{cases} \tag{56}$$

The two-stage association constraints are included as:

$$\begin{cases} -R_i^{\max} \le p_{sik} - p_{ik} \le R_i^{\max} \\ -R_j^{\max} \le p_{sjk} - p_{jk} \le R_j^{\max} \end{cases} \tag{57}$$

$$\begin{cases} -P_i^{RD} \le p_{si,k} - p_{si,k-1} \le P_i^{RU} \\ -P_j^{RD} \le p_{sj,k} - p_{sj,k-1} \le P_j^{RU} \end{cases} \tag{58}$$

where $R_i^{\max}$, $R_j^{\max}$ is the reserve upper limit for the thermal power unit and CHP unit respectively, P_i^{RU}, P_i^{RD}, P_j^{RU}, P_j^{RD} is the maximum climbing slope of the unit.

C. SOLUTION

As for the solving complexity, the SEED problem of UIHPS considering IDR developed by the above model is a mixed linear integer programming (MLIP) problem, including the amount of binary variables:

$$K(4 + S)(I + J) \tag{59}$$

the amount of continuous variables:

$$K(1 + S)(3INL_i + 3JNL_m + JNL_mNL_n + W + PV + 2U + NL_p + 1) \tag{60}$$

the amount of constraints:

$$K(1 + S)(9I + 13J + INL_i + INL_n + JNL_i + JNL_m + W + PV + 3U + 2NL_p + 3 + 1/K) \tag{61}$$

Which can be solved by commercial solver conveniently. In this paper, the MILP problem is formulated by matlab2018a, and solved by cplex12.8 on a laptop with intel i5 2.3Ghz quad-cores processor and 16GB RAM.

VI. CASE STUDY

A. CASE SETTING

In order to verify the effectiveness of the proposed SEED strategy, a test system consisting of an ieee34 node power system [57] and a 26-node thermal system [58] is established, which is located in an urban area divided into five residential areas. The test system includes 5 TPP (TPP1–TPP5), 3 CHP (CHP1–CHP3), 1 suburban wind farm and 1 urban photovoltaic power station. The electric heating load of the system participates in IDR under the management of two IERs. Users under two IER management have different preference costs and preference loads. The corresponding topological structure of the system is shown in Fig. 5(a). The geographic location of each unit and the center of each residential area is marked in Fig. 5(b), where the population PO_f of Area 1 ∼ Area 5 is 3.4*10^5, 2.6*10^5, 4*10^5, 2.8*10^5, 2.7*10^5, respectively.

The topological data of the thermal system are from [58]. Units' operation and emission parameters are given in Table 6–9. The user's direct electrical and thermal load demand and preference load are given in Fig. 12 and Table 10. The thermal energy price is assumed to be 300 RMB/MWh. The IDR electricity price adjustment interval is assumed to be 700 ∼ 1600 RMB/MWh. The user's electrothermal conversion equipment capacity upper limit is set to 50% of the heat demand. Points 6, 7, and 8 represent the location of the CHP units, which are both in densely populated areas.

Human settlement pollution costs per hour of primary PM2.5 (PR^{AP}) provided by smart environmental sensing [59], [60] is 0.05 RMB and the secondary PM2.5 hazard weight factor ς is taken as 1. The mean of the wind and light scenarios generated by the Monte Carlo simulation was formulated as the wind and solar predictions shown in Table 11 and 12, with the standard deviation set to 30% of the predicted value. Reduce the number of scenarios to $N_s = 9$, the probability of occurrence is 0.36, 0.15, 0.15, 0.09, 0.09, 0.0625, 0.0375, 0.0375, 0.0125, separately. Under heavy fog, the PV maintenance cost is set to 100 RMB/MW, and the maintenance

TABLE 4. Results.

	Economic benefit (RMB)	Total pm2.5 emissions (kg)	Cumulative PMGLC ($\mu g/m^3$)	Cumulative SPMGLC ($\mu g/m^3$)	Cumulative PPMGLC ($\mu g/m^3$)	Peak PMGLC ($\mu g/m^3$)	Peak SPMGLC ($\mu g/m^3$)
Case1	6578541	635.1	113.4	65.2	48.2	18.8	10.3
Case2	7202093	584.3	154.9	92.4	62.5	25.8	14.6
Case3	6898445	542.6	179.1	108.1	71	28.9	16.4
Case4	7276918	587.3	169.2	101.6	67.6	27.8	15.9
Case5	6521273	633.3	156.3	93.0	63.3	27.0	15.4
Case6	6630965	593.5	162.2	96.7	65.5	27.1	15.5

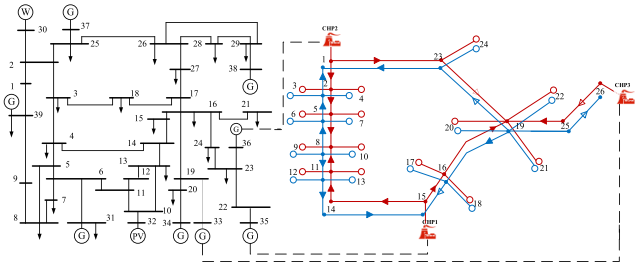

(a) Grid and heat network topology

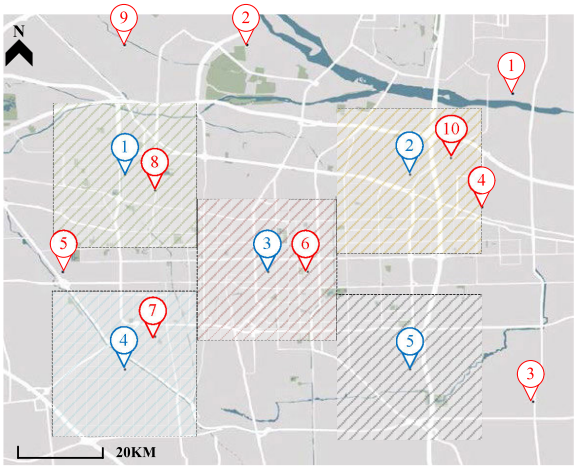

(b) Geographical distribution of units and residential areas

FIGURE 5. Test system.

cost of wind power is set to 120 RMB/MW. According to Chinese national standards [54] and study capacity, ET^{pm}_{lim} is set to 645.8kg. The background concentration, atmospheric stability, ABL height and other data of various pollutants within 24 hours of the dispatch cycle are given in Fig. 13 and Table 13–14 respectively, taken from the data of a typical winter day in a city from the northern China captured by smart environmental sensing platform [61].

We use the proposed method as Case 1 and compare it with 5 other cases in two groups to illustrate the effectiveness of the proposed method. The settings for each case are shown in Table 3 Each set of cases considers environmental optimization goals based on optimizing economic benefits. In Case 2, PPMGLC is optimized, without considering SPMGLC; In Case 3, the total PM2.5 emissions were optimized, without considering hazard caused by GLC of PM2.5; and in Case 4, only the economic profit was optimized, without considering any hazard of PM2.5. In cases 5 and 6, regardless of the IDR, SPMGLC is considered or not respectively on the basis of considering PPMGLC.

The first group comparison is set including Case 1, Case 2, Case 3, and Case 4, whose purpose is to analyze the impact of SPMGLC and PPMGLC in the dispatch target. The second group comparison is set including Case 1, Case 2, Case 5, and Case 6, whose purpose is to analyze the validity of the IDR constraint set and its relationship with SPMGLC in the objective function.

B. COMPARISON OF THE FIRST GROUP CASES: THE CONSIDERATION OF THE EFFECTIVENESS OF SPMGLC

The calculation results of the four cases in the first group are shown in Table 4. The economic benefit is the net economic benefit of ISO in the UIHPS through energy supply. The total PM2.5 emissions refer to the total amount of PM2.5 initially discharged by all units within 24 hours. Cumulative PMGLC and SPMGLC refer to the sum of the average PMGLC and SPMGLC of each hour of the city in the dispatch cycle, respectively, which can characterize the degree of health hazard accumulated by residents from PM2.5 caused by unit emissions. Peak PMGLC and SPMGLC refer to the maximum value of the hourly average concentration of PMGLC and SPMGLC in the dispatch period, respectively, which can characterize the maximum health hazard that residents continue to suffer in a short period of time.

1) The secondary PM2.5 generation and diffusion model established in this paper is effective. From the ratio of accumulated SPMGLC and accumulated PMGLC in the results of Table 4, the secondary PM2.5 accounted for 57.15%, 59.65%, 60.35%, and 60.07% of the total PM2.5 concentration in the four cases. This result is similar to the conclusion that the secondary aerosol accounts for 58% of the PM2.5 mass concentration in [31], [32], which can prove the validity of the secondary PM2.5 generation and diffusion model established in this paper in engineering calculation.

2) The SEED strategy proposed in this paper considering SPMGLC has a comprehensive and effective PM2.5 health hazard reduction benefit. Compared with Case 4, which only considers economic dispatch, Case 3 obtained a total reduction of 7.61% of total emissions through total control, but obtained the worst PMGLC and SPMGLC results, indicating that the reduction of PMGLC or SPMGLC cannot be

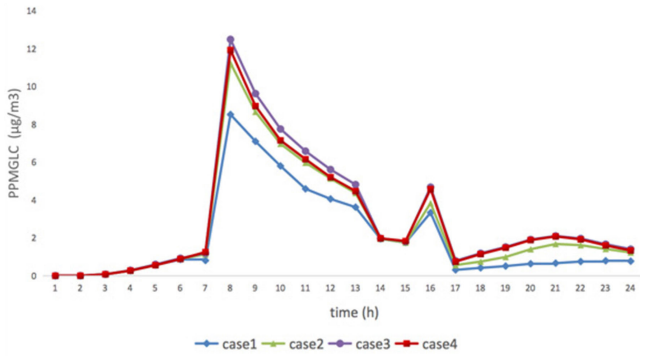

(a) PPMGLC

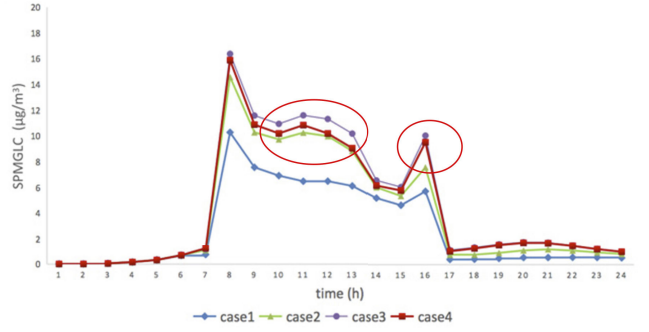

(b) SPMGLC

FIGURE 6. Time distribution of average PPMGLC and SPMGLC in each case.

achieved solely by controlling the total amount of initial pollutants. It is necessary to consider the diffusion law of PM2.5 and the generation law of secondary PM2.5 caused by meteorological conditions and geographical distribution of the units. Case 2 only included PPMGLC into the objective function, which resulted in a decrease of 8.42% in PMGLC and 9.07% in SPMGLC, which indicates that since the output and diffusion of different pollutants are positively correlated with unit output. the dispatch strategy only considering PPMGLC can affect the output of the units, and at the same time, it will bring emission reduction benefits to the GLC of the secondary PM2.5 precursors such as SO2 and NOX, which will bring about a certain reduction effect on SPMGLC. However, since Case 3 does not consider the nonlinear diffusion relationship between the generation and diffusion of the secondary PM2.5 precursor, the secondary PM2.5 generation process and the emission and diffusion of PM2.5, the reduction of SPMGLC and total.

3) PMGLC is limited. After comparison, the PMGLC and SPMGLC of Case 4 considering SPMGLC emission reduction were further reduced by 26.8% and 29.4% compared with Case 3, respectively, which has a more comprehensive and effective GLC emission reduction effect was achieved. At the same time, the peak PMGLC and the peak SPMGLC exhibit the same variation characteristics as the cumulative value, and Case 1 achieves the best reduction result, which shows that the proposed strategy has better PM2.5 health hazard reduction benefits in both cumulative and transient hazards.

4) It should be noted that the dispatch strategy considering SPMGLC proposed in this paper has lower economic profit than the dispatch strategy only considering PPMGLC, which still meets the total PM2.5 emission limitation (the total emission is less than the national standard of 645.8kg) and has a poor total PM2.5 emission benefit. From the comparison of Case 1, Case 2 and Case 4, Case 2 achieves 8.42% PMGLC reduction benefit with 1.03% gain loss, while total PM2.5 emissions in Case 3 are 0.51% less than Case 4. The cost of reducing the benefit of Case 1 by 32.97% in PMGLC is 9.59% loss of revenue and 8.14% initial emission increase. The cost performance of the proposed method in terms of economic profit and total emissions benefits needs further study.

5) Figure 6 shows the time distribution of the average PPMGLC and SPMGLC for the four cases in the first set of comparisons. By comparison of SPMGLC and PPMGLC, it can be found that: (1) SPMGLC is significantly lower than PPMGLC during 1:00–7:00 and 17:00–24:00 at night, and SPMGLC is significantly higher than PPMGLC during daytime. (2) There are different trends in the period from 10–13am: SPMGLC shows an increasing trend and PPMGLC continues to decay. (3) At 14:00–16:00, the trends of PPMGLC and SPMGLC are the same, but the ratio of SPMGLC to its peak value is significantly higher. These phenomena are caused by the influence of the light intensity on the generation of the secondary PM2.5, which is slow at night, peak at noon, and maintained at a high level in the evening due to the secondary generation. These features have a significant impact on the dispatch of the units and the implementation of the NSG system, especially for the comparison of Case 1 and Case 2.

Figure 7 shows the electrical output of each units in Case 1 and Case 2 (in the case of scenario 1, the probability of occurrence is 0.36). Fig. 8 shows the IDR real-time electricity price (IDREP) generated by the NSG and the actual thermal load of the user compared with the initial heat demand. It shows that: (1) In the period of low IDREP of ISO, users tend to use electric load to meet thermal energy demand, while in the period of higher electricity price, users significantly reduce the proportion of electric heating to reduce cost, indicating the validity of IDR related constraints in the SEED model. (2) The operation of the units is jointly analyzed with the SPMGLC time distribution. In order to cope with the impact of the secondary PM2.5 generation at noon and evening, considering the time lag of pollutant diffusion, Case 1 reduces the electrical output of TPP1, TPP4 in the upwind direction and CHP1, CHP2, CHP3 in the city center at 10–12 am and 14–15 pm compared to Case 2. At the same time, ISO significantly lowers the real-time electricity price in the period of 7:00–12:00, 14:00–15:00, and guided the user to purchase the electric energy through the IDR to realize the heat demand, so that the strategy of Case 1 was closed on the basis of CHP1 at 11:00–15:00, further CHP2 is turned off at 6:00–10:00, and CHP3 is turned off at 15:00–17:00. Then the CHP thermal output and electric output in the city

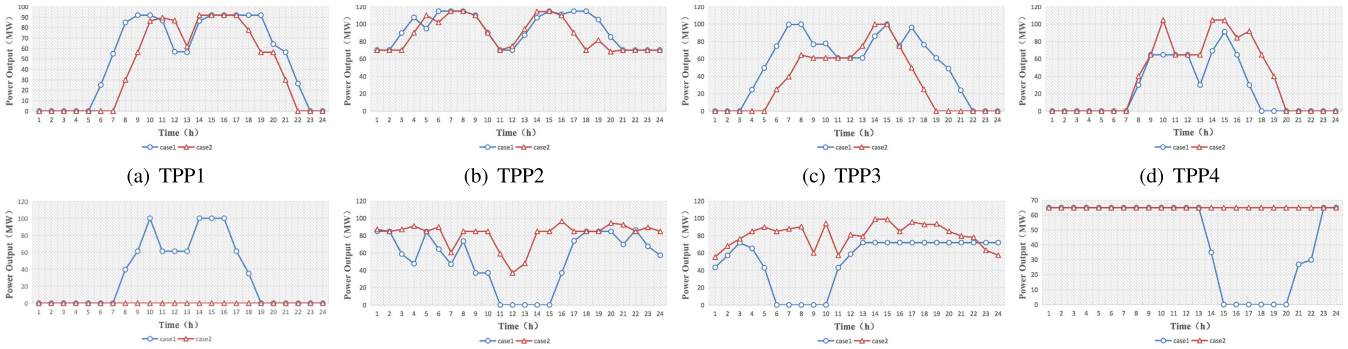

(a) TPP1 (b) TPP2 (c) TPP3 (d) TPP4

(e) TPP5 (f) CHP1 (g) CHP2 (h) CHP3

FIGURE 7. The power output of the units in Case 1 and Case 2 (Scenario 1).

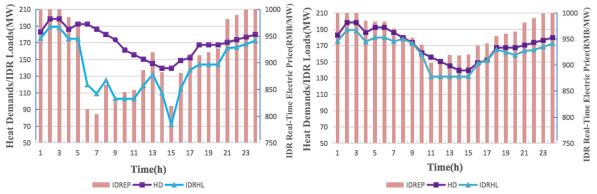

(a) Case 1 (b) Case 2

FIGURE 8. IDR situation under Nash equalization (Scenario 1).

center are more transferred to the electric power of TPP3 and TPP5 located in the downwind direction, further reducing SPMGLC and PPMGLC of the high-density residential area.

Figure 9 shows the urban PMGLC distribution at 11:00 in Case 1 and Case 2 respectively (in the case of scenario 1, the probability of occurrence is 0.36), in which the PMGLC near TPP4 and three CHPs of Case 1 are significantly lower than that of Case 2, and concentrations near TPP3 and TPP5 of Case 1 are higher than that of Case 2, which can confirm the dispatch process shown in Fig. 7–8, thus further illustrating the effectiveness of the proposed method in reducing SPMGLC and PMGLC and improving PM2.5 comprehensive hazards.

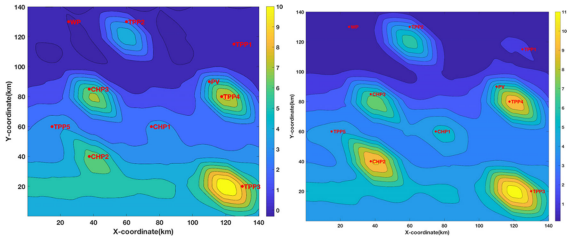

(a) Case 1 (b) Case 2

FIGURE 9. Distribution of urban PMGLC at 11:00 (Scenario 1).

C. COMPARISON OF THE SECOND GROUP CASES: ANALYSIS OF THE SYNERGY BETWEEN IDR AND SPMGLC CONTROL

Based on the analysis of the validity of the IDR in SEED in B, the efficiency of considering the IDR in the constraint condition and considering the SPMGLC in the objective function is further analyzed. In Table 4, the comparison of the two paths of Case 6 → Case 2 → Case 1 and Case 6 → Case 5 → Case 1 shows that only the introduction of IDR in SEED and the introduction of only SPMGLC can produce PPMGLC and SPMGLC reduction benefits, but the effect is very limited;

Based on the Case 6 results, only SPMGLC is introduced to generate 3.61% PMGLC reduction and 3.81% SPMGLC reduction, while only introducing IDR brought 4.46% PMGLC reduction and 4.42% SPMGLC reduction. The effect is much lower than considering both SPMGLC and IDR, which results in a 30.07% PMGLC reduction and a 32.55% SPMGLC reduction.

At the same time, the introduction of IDR alone results in a 9.37% increase in ISO revenue, a 0.55% reduction in total emissions, and a peak PMGLC reduction of 4.66%. The benefits of introducing only SPMGLC in these areas are reversed or not significant. The comparison between Case 5 and Case 1 can also show that the introduction of IDR based on SPMGLC can greatly reduce the effect of PM2.5 concentration reduction while reducing the economic loss and total emission reduction caused by SPMGLC control.

According to the thermal output of each CHP unit in the four cases shown in Fig. 10 (taking Scenario 1 as an example, the probability of occurrence is 0.36), the mechanism of interaction between IDR and SPMGLC is further analyzed. Based on Case 6, the operating conditions of Case 5 and Case 2 is compared: unit heat output change of Case 2 is usually significantly higher than that of Case 5, but the trend of the two periods of 10:00–15:00 and 18:00–22:00 is reversed. At the same time, comparing the operating state changes of Case 1 and Case 5, it can be found that Case 1 has a significant change in the amount of change based on the same trend as Case 5. This phenomenon is due to the fact that in the absence of IDR, the CHP unit has only limited operating space because of the need to meet thermal load balancing constraints. The introduction of IDR brings the possibility of replacing the heat load with the electric load to replace the heat load, so that the thermal output and the electric output of the CHP are further decoupled, and the operating range can be adjusted according to the capacity of the IDR, thereby having a significantly expanded operating space. When targeting only economics and PPMGLC,

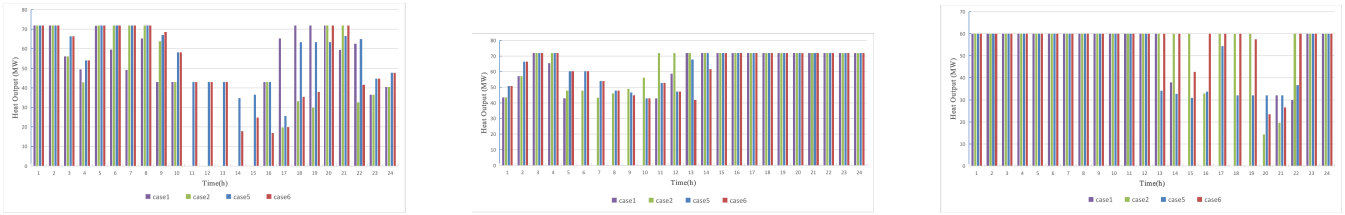

(a) CHP1 (b) CHP2 (c) CHP3

FIGURE 10. CHP unit heat output in different cases (Scenario 1).

the expanded operating space is mainly adjusted based on improved economic indicators. Considering SPMGLC and PPMGLC in the objective function can guide the CHP unit to adjust the state in the direction of facilitating the mitigation of PM2.5 in the extended operating space. In the case where the CHP unit is in the center of the city, the significance of the interaction between IDR and SPMGLC is more significant.

D. FURTHER ANALYSIS

1) SPMGLC GOVERNANCE CONSIDERS THE WEIGHT OF THE PRICE

According to the case analysis in above, it is necessary to further explore the additional cost and additional emissions caused by the cumulative value of SPMGLC and peak reduction. In Case 1, the unit human settlement pollution costs of the secondary PM2.5 is gradually increased from 0.005RMB/h to 0.05RMB/h, which is equivalent to gradually increasing the human health hazards weight factor of secondary PM2.5 from 0.1 to 1. The relationship of SPMGLC cumulative value and peak value with economic benefit loss and additional initial emissions was calculated separately, resulting in a sensitivity curve as shown in Fig. 11.

Figure 11 shows that the relationship between the cumulative value, the peak value of SPMGLC and economic benefit loss, the additional primary emissions present a similar piecewise linear feature. The cost performance of SPMGLC control is worsening with the improvement of the reduction effect, but there is a balance point effect: the SPMGLC cumulative value is reduced by 21.2% compared with the result of Case 2 and the peak SPMGLC is reduced by 27.4% compared with the result of Case 2, the cost performance of the SPMGLC control is relatively balanced, when the unit human settlement pollution cost is set to 0.016 RMB/h. The above results show that when public utilities formulate environmental economic cost parameters, they need to focus on the analysis of the balance point of environmental management cost performance as a policy reference.

2) CHANGES IN USER PREFERENCE COSTS IN IDR

We analyzed the relationship between the user preference cost and the dispatch result set in the contract signed by the IER and the user in the NSG mechanism And the results are shown in Table 5. The increase in preference costs will worsen PMGLC and increase the economic profit of ISO;

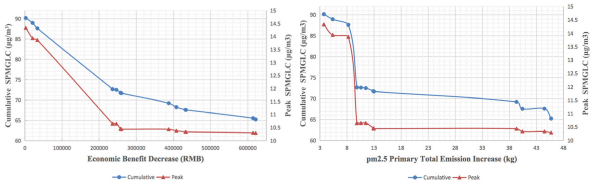

(a) Economic benefit loss (b) Additional Total PM2.5 emissions

FIGURE 11. Sensitivity analysis of cost-effectiveness of SPMGLC reduction.

the reduction in preference costs will reduce the benefits of PMGLC while reducing the economic profit of ISO. The change of preference cost will lead to the increase of initial emission increment. PMGLC, economic income and total initial emissions are more sensitive to the decrease of preference cost. The peak PMGLC and SPMGLC are mainly affected by the maximum output moment of the units, and the demand response price does not affect the peak concentration of pm2.5. The above conclusions can be used as a reference for the development of IDR parameters.

VII. CONCLUSION

A SEED model of UIHPS considering the effects of IDR and secondary PM2.5 is proposed in this paper to mitigate the primary and secondary PM2.5 human health hazards caused by urban energy generation. Smart environmental sensing provides some data support for the UIHPS.The relevant conclusions are as follows:

1) The constructed secondary PM2.5 generation and diffusion function for dispatch can effectively simulate the contribution of UIHPS to the secondary PM2.5 hazard. In PMGLC caused by UIHPS emissions, the contribution of secondary PM2.5 accounts for 57% - 60%. The secondary PM2.5 shows a different characteristic from the primary PM2.5 in terms of TSD which has a significant impact on the dispatch results of the units.

2) Constraint set of IDR in the SEED model can reflect the balance of both gamers' interests, which effectively guide users to help realize the transfer of CHP's PM2.5 hazard by adjusting the electric load and heating load, and reflect the influence of user side participation on reducing PM2.5 hazard.

3) Compared with the model only considers the economy, only considers economy and PPMGLC, only considers the economy, and only considers PM2.5 total emissions, using

TABLE 5. Results under different preference costs.

	Economic benefit (RMB)	Total PM2.5 emissions (kg)	Cumulative PMGLC (μg/m^3)	Cumulative SPMGLC (μg/m^3)	Peak PMGLC (μg/m^3)	Peak SPMGLC (μg/m^3)
Preference cost -10%	6505680	635.7	112.7	64.8	18.8	10.3
Preference cost -5%	6558400	635.2	113.3	65.2	18.8	10.3
Case1	6578541	635.1	113.4	65.2	18.8	10.3
Preference cost $+5\%$	6583115	635.1	113.6	65.3	18.8	10.3
Preference cost $+10\%$	6814416	635.9	118.5	67.3	18.8	10.3

the proposed model in this paper, both SPMGLC and PMGLC can be significantly reduced, and the alleviation of the comprehensive hazards of PM2.5 was more than 30%. Although with relatively low economic benefits and increased PM2.5 total emissions, the proposed method's PMGLC reduction ratio is much higher than the economic income reduction ratio, while the total emission constraints effectively ensure that the total PM2.5 emissions of the proposed model still meet the requirements of the Chinese national standards for special emission limits.

4) Considering the SPMGLC function in the objective function have a significant mutual promotion effect with the introduction of the IDR constraint set in the constraints. The IDR constraint set expands the adjustment space of the CHP unit, while the inclusion of the SPMGLC into the objective function can guide the CHP unit to adjust the operating state by using the expanded operating space in a direction which is beneficial to mitigate the PM2.5 integrated hazard.

The follow-up will further study this issue from the perspective of multi-objective optimization, data-driven method [62]–[64], and study the role of more comprehensive energy demand side resources such as industrial load, energy storage, and electric vehicles [65].

APPENDIXES

APPENDIX A
THE MODEL OF UNITS

A. TPP OPERATING CONSTRAINTS

$$\begin{cases} v_{i,k-1} - v_{i,k} + \omega_{ik}^{on} + \omega_{ik}^{off} = 0 \\ \omega_{ik}^{off} + \omega_{ik}^{on} \le 1 \\ v_{ik}, \omega_{ik}^{off}, \omega_{ik}^{on} \in \{0, 1\} \end{cases} \tag{A1}$$

$$\underline{P_i} v_{ik} \le p_{ik} \le \overline{P_i} v_{ik} \tag{A2}$$

$$-P_i^{RD} \le p_{i,k} - p_{i,k-1} \le P_i^{RU} \tag{A3}$$

(A1) is a binary variable constraint, (A2) is the unit output constraint, and (A3) is the ramping constraint. Where $\underline{P_i}\overline{P_i}$ is the upper and lower limits of the unit output. $\omega_{ik}^{on}\omega_{ik}^{off}$ are shut-down and start-up indicator of unit respectively.

B. CHP OPERATING CONSTRAINTS

$$\begin{cases} v_{j,k-1} - v_{j,k} + \omega_{jk}^{on} + \omega_{jk}^{off} = 0 \\ \omega_{jk}^{off} + \omega_{jk}^{on} \le 1 \\ v_{jk}, \omega_{jk}^{off}, \omega_{jk}^{on} \in \{0, 1\} \end{cases} \tag{A4}$$

TABLE 6. Parameters of photovoltaic and wind power generator.

$P_{pv,STC}$ (KW)	T_{pvop} (°C)	CPV	N_{PVM}
230	43	0.00122	2000
P_w^R (MW)	ws_w^R (km/h)	ws_w^{in} (km/h)	ws_w^{out} (km/h)
100	48.6	12.6	90

$$-P_j^{RD} \le p_{j,k} - p_{j,k-1} \le P_j^{RU} \tag{A5}$$

(A4) is the binary variable constraint, and (A5) is the unit's electrical output ramping constraint.

C. UNIT EMISSIONS MODEL CONSIDERING POLLUTANT EMISSION REDUCTION MEASURES

1) ORIGINAL EMISSIONS WITHOUT CONSIDERING EMISSION REDUCTION MEASURES

When pollution control measures are not considered, the primary pollutant emissions from coal-fired units are generally modeled as a quadratic function of output:

$$es_{ik}^{PM} = v_{ik}[aa_i^{PM} + ba_i^{PM} p_{ik} + ca_i^{PM} p_{ik}^2] \tag{A6}$$

$$es_{ik}^{SO_2} = v_{ik} aa_i^{SO_2}[ac_i + bc_i p_{ik} + cc_i p_{ik}^2] \tag{A7}$$

$$es_{ik}^{NO_x} = v_{ik}[aa_i^{NO_x} + ba_i^{NO_x} p_{ik} + ca_i^{NO_x} p_{ik}^2] \tag{A8}$$

where es_{ik}^{PM}, $es_{ik}^{SO_x}$, and $es_{ik}^{NO_x}$ are the total amount of PM2.5, SO_2, NO_x originally discharged by the unit i during the period k, ac_i, bc_i, cc_i is the unit fuel cost parameter, aa_i, ba_i, ca_i etc. are the emission factors (or fuel conversion factor) of the corresponding pollutants.

The original emission model of the TPP is sectionally linearized as:

$$es_{ik}^{SO_2} = A_i^P v_{ik} + \sum_{\ell p}^{NL_i} PL_{ik\ell p}^{SO_2} \delta_{ik\ell p}^P \tag{A9}$$

$$es_{ik}^{NO_x} = A_i^P v_{ik} + \sum_{\ell p}^{NL_i} PL_{ik\ell p}^{NO_x} \delta_{ik\ell p}^P \tag{A10}$$

$$es_{ik}^{pm2.5} = A_i^P v_{ik} + \sum_{\ell p}^{NL_i} PL_{ik\ell p}^{pm2.5} \delta_{ik\ell p}^P \tag{A11}$$

The pollutant emission model of CHP units based on linear superposition modeling of corner points using the material

TABLE 7. Parameters of CHP1–2.

m	Q_{jm}^{m} (MW)	P_{jm}^{m} (MW)	cc_{jm}^{CHP} (t)	aa_{jm}^{PM} (kg)	$aa_{jm}^{NO_x}$ (kg)	$aa_{j}^{SO_2}$ (kg/t)	z_j^e (m)
1	0	45	28.35	35.1	230.23	1.32	150
2	43	37	33.81	41.8	274.57		
3	72	85	61.32	75.9	497.98		
4	0	100	44.52	55.1	361.54		

TABLE 8. Parameters of CHP3.

m	Q_{jm}^{m} (MW)	P_{jm}^{m} (MW)	cc_{jm}^{CHP} (t)	aa_{jm}^{PM} (kg)	$aa_{jm}^{NO_x}$ (kg)	$aa_{j}^{SO_2}$ (kg/t)	z_j^e (m)
1	0	32	19.32	35.1	156.89	1.25	250
2	32	27	17	20.8	136.43		
3	60	65	34.65	42.9	281.39		
4	0	75	24.15	29.9	196.12		

TABLE 9. Parameters of the TPP.

i	ac_i (t/MW^2*h)	bc_i (t/MW*h)	cc_i (t/h)	$aa_i^{NO_x}$ (kg/MW^2*h)	$ba_i^{NO_x}$ (kg/MW*h)	$ca_i^{NO_x}$ (kg/h)
1	6.55E-05	0.327	15.199	2.94E-04	1.94	35.53
2	1.01E-04	0.342	11.556	2.44E-04	1.9	34.91
3	7.54E-05	0.329	14.557	3.00E-04	1.9	43.38
4	5.59E-05	0.328	18.857	2.66E-04	1.68	38.46
5	5.08E-05	0.344	23.197	2.95E-04	1.86	42.62
i	aa_i^{PM} (kg/MW^2*h)	ba_i^{PM} (kg/MW*h)	ca_i^{PM} (kg/h)	$aa_i^{SO_2}$ (kg/t)	z_i^e (m)	
1	4.63E-05	0.29	6.7	1.32	450	
2	4.58E-05	0.36	6.55	1.33	510	
3	5.53E-05	0.35	7.99	1.25	441	
4	3.97E-05	0.25	5.74	1.31	556	
5	5.46E-05	0.43	7.81	1.20	465	

TABLE 10. User preference electrical load under IER management (MW).

Time	1	2	3	4	5	6	7	8	9	10	11	12
IER1	159.1	169.9	179.9	199.3	209.6	209.6	229.3	238.9	248.7	283.1	307.8	307.5
IER2	134.1	134.9	134.9	134.3	134.6	134.6	159.3	308.9	308.7	308.1	207.8	207.5
Time	13	14	15	16	17	18	19	20	21	22	23	24
IER1	307.2	306.9	281.9	267.4	257.6	238.4	228.4	218.3	188.5	178.7	168.8	158.9
IER2	207.2	306.9	306.9	307.4	307.6	258.4	208.4	158.3	158.5	133.7	133.8	133.9

TABLE 11. Average light intensity (w/m2).

Time	1	2	3	4	5	6	7	8	9	10	11	12
BP_k^R	0	0	0	0	0	16	36	92	130	154	162	154
Time	13	14	15	16	17	18	19	20	21	22	23	24
BP_k^R	130	92	36	16	4	0	0	0	0	0	0	0

TABLE 12. Mean values of wind speed and wind direction.

Time	1	2	3	4	5	6	7	8	9	10	11	12
Speed (km/h)	1.69	1.8	2.16	1.69	2.41	3.24	3.24	2.41	2.41	1.8	2.41	1.33
dirction (°)	23	48	63	35	26	38	50	42	50	32	35	357
Time	13	14	15	16	17	18	19	20	21	22	23	24
Speed (km/h)	1.19	1.44	1.44	0.36	0.83	1.33	1.44	1.8	2.41	2.16	1.8	1.44
dirction (°)	35	18	96	98	100	109	116	123	135	134	145	153

core algorithm is described as (A12):

$$\begin{cases} es_{kj}^{NO_x} = \sum_{m}^{NL_m} \alpha_{kj}^{m} aa_{jm}^{NO_x} \\ es_{kj}^{SO_2} = \sum_{m}^{NL_m} \alpha_{kj}^{m} aa_{jm}^{SO_2} \\ es_{kj}^{PM} = aa_{j}^{PM} c_{kj}^{CHP} \end{cases} \tag{A12}$$

where C_{jm}^{CHP} is the corner fuel cost, $aa_{jm}^{NO_x}$, aa_{jm}^{PM} is the original discharge of corner point pollutants, and $aa_j^{SO_2}$ is the fuel conversion factor.

2) PRIMARY EMISSIONS CONSIDERING EMISSION REDUCTION MEASURES

Faced with severe environmental protection and policy requirements, many developing countries, especially China's

TABLE 13. Atmospheric stability.

t/h	1	2	3	4	5	6	7	8	9	10	11	12
ϖ	6	6	6	6	6	6	5	3	3	3	3	3
t/h	13	14	15	16	17	18	19	20	21	22	23	24
ϖ	3	2	2	3	5	6	6	6	6	6	6	6

TABLE 14. ABL height (m).

t/h	1	2	3	4	5	6	7	8	9	10	11	12
h/m	155	160	157	165	180	230	250	270	340	440	550	600
t/h	13	14	15	16	17	18	19	20	21	22	23	24
h/m	630	650	640	500	100	120	127	133	145	150	155	165

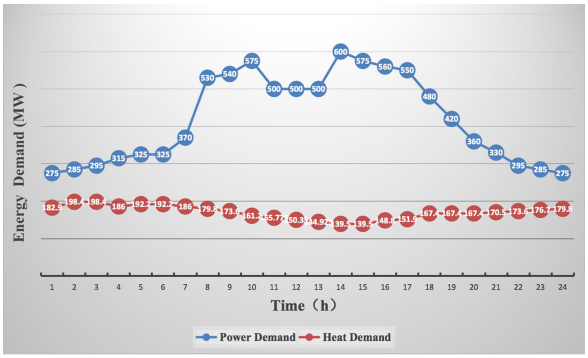

FIGURE 12. User's total electricity demand and heat demand.

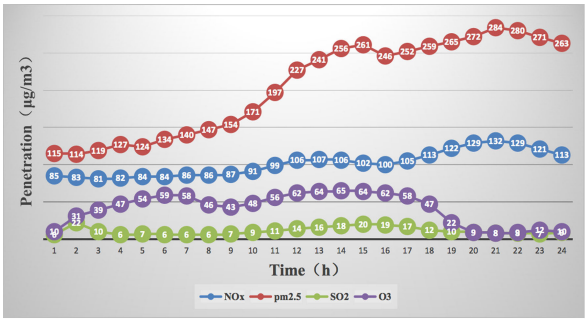

FIGURE 13. Background concentration of various atmospheric pollutants.

TG units and CHP units, have installed emission reduction devices for different pollutants, including electro static precipitator (ESP) system for PM2.5., flue gas desulfurization system (FGD) for SO_2 and selective catalytic reduction system (SCR) for NO_x, which is Modeled separately as follows:

FGD for SO_2 can be modeled as (A13). Where $e_i^{SO_2}$ is the quality of SO_2 after emission reduction by FGD, and μ^{SO_2} is the efficiency of SO_2 emission reduction, which is constant.

$$e_{ik}^{SO_2} = (1 - \mu_i^{SO_2}) \times es_{ik}^{SO_2} \tag{A13}$$

ESP for PM2.5 emission reduction can be modeled as (A14).

$$\begin{cases} e_{ik}^{pm2.5} = (1 - \mu_{sik}^{pm}) \times es_{ik}^{pm2.5} \\ \mu_{ik}^{pm2.5} = v^{PM} p_{ik} / \overline{p_i} + \mu_i^{pm2.5} \end{cases} \tag{A14}$$

SCR for NO_x emission reduction can be modeled as (A15). The operation of the SCR system is mainly based on the catalyst. When the units are running at low power output, the catalyst is degraded due to the low temperature [28]. At this time, the SCR system needs to be shut down, resulting in a significant increase in emissions.

$$e_{sik}^{NOx} = \begin{cases} (1 - \mu_i^{NOx}) \times es_{sik}^{NO_x} & (\overline{P_i} \geq p_{sik} \geq P_{i,1}) \\ es_{sik}^{NO_x} & (\underline{P_i} \leq p_{sik} < P_{i,1}) \end{cases} \tag{A15}$$

where $P_{i,1}$ is the output threshold for closing the SCR, μ_i^{NOx} is the efficiency of NO_x emission reduction.

The model of the CHP emission model considering the emission reduction measures is the same as TPP's except that the index i should be changed to j.

(A15) can be linearized as (A16), where M is a large number, and $sign_{ik}$ is a binary variable indicating the interval in which the unit output is located: when $\overline{P_i} \geq p_{sik} \geq P_{i,1}$, $sign_{ik} = 0$; when $\underline{P_i} \leq p_{sik} < P_{i,1}$, $sign_{ik} = 1$.

$$\begin{cases} e_{ik}^{NOx} - es_{ik}^{NO_x} + M(1 - sign_{ik}) \geq 0 \\ e_{ik}^{NOx} - [(1 - \mu_i^{NOx}) \times es_{ik}^{NO_x}] + M sign_{ik} \geq 0 \end{cases} \tag{A16}$$

APPENDIX B
DATA OF SIMULATIONS

See Figures 12 and 13 and Tables 6–14.

REFERENCES

[1] C. Song, L. Wu, and Y. Xie, "Air pollution in China: Status and spatiotemporal variations," *Environ. Pollut.*, vol. 227, no. 8, pp. 334–347, 2017.
[2] S. Wan, Z. Gu, and Q. Ni, "Cognitive computing and wireless communications on the edge for healthcare service robots," *Comput. Commun.*, vol. 149, no. 1, pp. 99–106, 2019.
[3] W. Li, X. Liu, and J. Liu, "On improving the accuracy with auto-encoder on conjunctivitis," *Appl. Soft Comput.*, vol. 81, no. 8, 2019, Art. no. 105489.
[4] Y. Zhao, H. Li, S. Wan, A. Sekuboyina, X. Hu, G. Tetteh, M. Piraud, and B. Menze, "Knowledge-aided convolutional neural network for small organ segmentation," *IEEE J. Biomed. Health Inform.*, vol. 23, no. 4, pp. 1363–1373, Jul. 2019.
[5] H. Zheng, S. Kong, and Q. Yan, "The impacts of pollution control measures on PM2. 5 reduction: Insights of chemical composition, source variation and health risk," *Atmos. Environ.*, vol. 197, no. 1, pp. 103–117, 2019.
[6] Y. S. Wang, L. Yao, and L. L. Wang, "Mechanism for the formation of the January 2013 heavy haze pollution episode over central and eastern China," *Sci. China Earth Sci.*, vol. 57, no. 1, pp. 14–25, 2014.
[7] X. Wu, Y. Ding, and S. Zhou, "Temporal characteristic and source analysis of PM2. 5 in the most polluted city agglomeration of China," *Atmos. Pollut. Res.*, vol. 9, no. 6, pp. 1221–1230, 2018.

[8] J. Xing, S. X. Wang, and S. Chatani, "Projections of air pollutant emissions and its impacts on regional air quality in China in 2020," *Atmos. Chem. Phys.*, vol. 11, no. 7, pp. 3119–3136, 2011.

[9] H. Falsafi, A. Zakariazadeh, and S. Jadid, "The role of demand response in single and multi-objective wind-thermal generation scheduling: A stochastic programming," *Energy*, vol. 64, Jan. 2014, Art. no. 853G867.

[10] Q. Lu, S. Lü, and Y. Leng, "A Nash-Stackelberg game approach in regional energy market considering users' integrated demand response," *Energy*, vol. 175, no. 5, pp. 456–470, 2019.

[11] J. Wang, H. Zhong, Z. Ma, Q. Xia, and C. Kang, "Review and prospect of integrated demand response in the multi-energy system," *Appl. Energy*, vol. 202, pp. 772–782, Sep. 2017.

[12] Y. Yin, L. Chen, and Y. Xu, "QoS prediction for service recommendation with deep feature learning in edge computing environment," *Mobile Netw. Appl.*, to be published, doi: 10.1007/s11036-019-01241-7.

[13] H. Gao, W. Huang, X. Yang, Y. Duan, and Y. Yin, "Toward service selection for workflow reconfiguration: An interface-based computing solution," *Future Gener. Comput. Syst.*, vol. 87, pp. 298–311, Oct. 2018.

[14] C. Chen, J. Hu, T. Qiu, M. Atiquzzaman, and Z. Ren, "CVCG: Cooperative V2V-aided transmission scheme based on coalitional game for popular content distribution in vehicular ad-hoc networks," *IEEE Trans. Mobile Comput.*, vol. 18, no. 12, pp. 2811–2828, Dec. 2018.

[15] J. K. Delson, "Controlled emission dispatch," *IEEE Trans. Power App. Syst.*, vol. PAS-5, no. 5, pp. 1359–1366, Sep. 1974.

[16] L. Wu, M. Shahidehpour, and T. Li, "Stochastic security-constrained unit commitment," *IEEE Trans. Power Syst.*, vol. 22, no. 2, pp. 800–811, May 2007, doi: 10.1109/TPWRS.2007.894843.

[17] M. J. Ghadi, A. I. Karin, and A. Baghramian, "Optimal power scheduling of thermal units considering emission constraint for GENCOs' profit maximization," *Int. J. Elect. Power Energy Syst.*, vol. 82, no. 11, pp. 124–135, 2016.

[18] Z. Geng, A. J. Conejo, and Q. Chen, "Power generation scheduling considering stochastic emission limits," *Int. J. Elect. Power Energy Syst.*, vol. 95, no. 2, pp. 374–383, 2018.

[19] Z. Geng, Q. Chen, Q. Xia, D. S. Kirschen, and C. Kang, "Environmental generation scheduling considering air pollution control technologies and weather effects," *IEEE Trans. Power Syst.*, vol. 32, no. 1, pp. 127–136, Jan. 2017.

[20] Y. Zhu, J. Wang, and B. Qu, "Multi-objective economic emission dispatch considering wind power using evolutionary algorithm based on decomposition," *Int. J. Elect. Power Energy Syst.*, vol. 63, no. 12, pp. 434–445, 2014.

[21] A. Y. Abdelaziz, E. S. Ali, and S. M. A. Elazim, "Combined economic and emission dispatch solution using flower pollination algorithm," *Int. J. Elect. Power Energy Syst.*, vol. 80, no. 9, pp. 264–274, 2016, doi: 10.1016/j.ijepes.2015.11.093.

[22] M. T. Tsay, "Applying the multi-objective approach for operation strategy of cogeneration systems under environmental constraints," *Int. J. Elect. Power Energy Syst.*, vol. 25, no. 3, pp. 219–226, 2003.

[23] H. R. Sadeghian and M. M. Ardehali, "A novel approach for optimal economic dispatch scheduling of integrated combined heat and power systems for maximum economic profit and minimum environmental emissions based on benders decomposition," *Energy*, vol. 102, pp. 10–23, May 2016.

[24] X. Wang, S. Chen, and Y. Zhou, "Optimal dispatch of microgrid with combined heat and power system considering environmental cost," *Energies*, vol. 11, no. 10, p. 2493, 2018.

[25] L. Wang, H. Zhen, X. Fang, S. Wan, W. Ding, and Y. Guo, "A unified two-parallel-branch deep neural network for joint gland contour and segmentation learning," *Future Gener. Comput. Syst.*, vol. 100, pp. 316–324, Nov. 2019.

[26] S. Lei, Y. Hou, and X. Wang, "Unit commitment incorporating spatial distribution control of air pollutant dispersion," *IEEE Trans. Ind. Informat.*, vol. 13, no. 3, pp. 995–1005, Jun. 2016.

[27] K.-C. Chu, M. Jamshidi, and R. E. Levitan, "An approach to on-line power dispatch with ambient air pollution constraints," *IEEE Trans. Autom. Control*, vol. AC-22, no. 3, pp. 385–396, Jun. 1977.

[28] D. Guo, J. Yu, and M. Ban, "Security-constrained unit commitment considering differentiated regional air pollutant intensity," *Sustainability*, vol. 10, no. 5, p. 1433, 2018.

[29] Y. Chen, T. Yu, and B. Yang, "Many-objective optimal power dispatch strategy incorporating temporal and spatial distribution control of multiple air pollutants," *IEEE Trans. Ind. Informat.*, vol. 15, no. 9, pp. 5309–5319, Sep. 2019.

[30] K. Qu, S. Shi, and T. Yu, "A convex decentralized optimization for environmental-economic power and gas system considering diversified emission control," *Appl. Energy*, vol. 240, no. 4, pp. 630–645, 2019.

[31] R. J. Huang, Y. Zhang, and C. Bozzetti, "High secondary aerosol contribution to particulate pollution during haze events in China," *Nature*, vol. 514, no. 7521, p. 218, 2014.

[32] R. Zhang, G. Wang, and S. Guo, "Formation of urban fine particulate matter," *Chem. Rev.*, vol. 115, no. 10, pp. 3803–3855, 2015.

[33] V. Dawar, B. Lesieutre, and T. Holloway, "An efficient approach to reduce emissions by coupling atmospheric and electricity market models," in *Proc. North Amer. Power Symp. (NAPS)*, 2012, pp. 1–6.

[34] J. S. Scire, D. G. Strimaitis, and R. J. Yamartino, "A user's guide for the CALPUFF dispersion model," Earth Tech., Concord, MA, USA, Tech. Rep. 10, 2000.

[35] Z. Geng, A. J. Conejo, and C. Kang, "Stochastic scheduling ensuring air quality through wind power and storage coordination," *IET Gener., Transmiss. Distrib.*, vol. 11, no. 8, pp. 2031–2040, 2017.

[36] Q. P. Zheng, J. Wang, and A. L. Liu, "Stochastic optimization for unit commitment—A review," *IEEE Trans. Power Syst.*, vol. 30, no. 4, pp. 1913–1924, Jul. 2015.

[37] N. Growe-Kuska, H. Heitsch, and W. Romisch, "Scenario reduction and scenario tree construction for power management problems," in *Proc. IEEE Bologna Power Tech Conf.*, vol. 3, Jun. 2003, p. 7.

[38] R. Zhang, P. Xie, and C. Wang, "Classifying transportation mode and speed from trajectory data via deep multi-scale learning," *Comput. Netw.*, vol. 162, 2019, Art. no. 106861.

[39] Z. Gao, H. Z. Xuan, and H. Zhang, "Adaptive fusion and category-level dictionary learning model for multi-view human action recognition," *IEEE Internet Things J.*, to be published.

[40] Y. Riffonneau, S. Bacha, F. Barruel, and S. Ploix, "Optimal power flow management for grid connected PV sytems with batteries,"' *IEEE Trans. Sustain. Energy*, vol. 2, no. 3, pp. 309–320, Jul. 2011.

[41] S. Hadayeghparast, A. S. Farsangi, and H. Shayanfar, "Day-ahead stochastic multi-objective economic/emission operational scheduling of a large scale virtual power plant," *Energy*, vol. 172, pp. 630–646, Apr. 2019.

[42] C. Chen, Q. Pei, and X. Li, "A GTS allocation scheme to improve multiple-access performance in vehicular sensor networks," *IEEE Trans. Veh. Technol.*, vol. 65, no. 3, pp. 1549–1563, Mar. 2016.

[43] L. Liu, C. Chen, T. Qiu, M. Zhang, S. Li, and B. Zhou, "A data dissemination scheme based on clustering and probabilistic broadcasting in VANETs," *Veh. Commun.*, vol. 13, pp. 78–88, Jul. 2018.

[44] M. Carrion and J. M. Arroyo, "A computationally efficient mixed-integer linear formulation for the thermal unit commitment problem," *IEEE Trans. Power Syst.*, vol. 21, no. 3, pp. 1371–1378, Aug. 2006.

[45] C. Chen, L. Liu, T. Qiu, Z. Ren, J. Hu, and F. Ti, "Driver's intention identification and risk evaluation at intersections in the Internet of vehicles," *IEEE Internet Things J.*, vol. 5, no. 3, pp. 1575–1587, Jun. 2018.

[46] Y. Yin, L. Chen, Y. Xu, and J. Wan, "Location-aware service recommendation with enhanced probabilistic matrix factorization," *IEEE Access*, vol. 6, pp. 62815–62825, 2018.

[47] J. Lelieveld, J. S. Evans, and M. Fnais, "The contribution of outdoor air pollution sources to premature mortality on a global scale," *Nature*, vol. 525, no. 7569, p. 367, 2015.

[48] Z. Liu, W. Gao, and Y. Yu, "Characteristics of PM 2.5 mass concentrations and chemical species in urban and background areas of China: Emerging results from the CARE-China network," *Atmos. Chem. Phys.*, vol. 18, no. 12, pp. 8849–8871, 2018.

[49] Y. Xu, Q. Liao, F. Tang, D. Liu, D. Ke, S. Peng, and Z. Yang, "Combined heat and power dispatch based on integrated demand response and heat transmission for wind power accommodation," in *Proc. IEEE Power Energy Soc. Gen. Meeting (PESGM)*, Aug. 2018, pp. 1–5.

[50] M. M. Yu and S. H. Hong, "A real-time demand-response algorithm for smart grids: A Stackelberg game approach," *IEEE Trans. Smart Grid*, vol. 7, no. 2, pp. 879–888, Mar. 2016.

[51] Y. Cheng, N. Zhang, and C. Kang, "Low-carbon economic dispatch for integrated heat and power systems considering network constraints," *J. Eng.*, vol. 2017, no. 14, pp. 2628–2633, 2017.

[52] S. Yao, W. Gu, and S. Lu, "A transient thermodynamic model of district heating network for operational optimization of the energy integration system," in *Proc. IEEE Conf. Energy Internet Energy Syst. Integr. (EI)*, Nov. 2017, pp. 1–6.

[53] G. Li, G. Li, and M. Zhou, "Model and application of renewable energy accommodation capacity calculation considering utilization level of inter-provincial tie-line," *Protection Control Mod. Power Syst.*, vol. 4, no. 4, pp. 1–12, 2019.
[54] *Emission Standard of Air Pollutants for Thermal Power Plants*, Standard GB13223-2011, 2011. [Online]. Available: http://kjs.mee.gov.cn/hjbhbz/bzwb/dqhjbh/dqgdwrywrwpfbz/201109/t20110921_217534.shtml
[55] L. Ma, N. Liu, J. Zhang, W. Tushar, and C. Yuen, "Energy management for joint operation of CHP and PV prosumers inside a grid-connected micro-grid: A game theoretic approach," *IEEE Trans. Ind. Informat.*, vol. 12, no. 5, pp. 1930–1942, Oct. 2016.
[56] M. J. Salehpour and S. M. M. Tafreshi, "Optimal bidding strategy for a smart microgrid in day-ahead electricity market with demand response programs considering uncertainties," in *Proc. Smart Grid Conf. (SGC)*, 2017, pp. 1–7.
[57] A. Pai, *Energy Function Analysis for Power System Stability*. Boston, MA, USA: Kluwer, 1989.
[58] X. Liu, J. Wu, N. Jenkins, and A. Bagdanavicius, "Combined analysis of electricity and heat networks," *Appl. Energy*, vol. 162, pp. 1238–1250, Jan. 2016.
[59] C. Chen, L. Liu, T. Qiu, K. Yang, F. Gong, and H. Song, "ASGR: An artificial spider-Web-based geographic routing in heterogeneous vehicular networks," *IEEE Trans. Intell. Transp. Syst.*, vol. 20, no. 5, pp. 1604–1620, May 2019.
[60] H. Gao, S. Mao, W. Huang, and X. Yang, "Applying probabilistic model checking to financial production risk evaluation and control: A case study of Alibaba's Yu'e Bao," *IEEE Trans. Comput. Social Syst.*, vol. 5, no. 3, pp. 785–795, Sep. 2018.
[61] *China Air Quality Online Monitoring and Analysis Platform*. Accessed: Aug. 26, 2019. [Online]. Available: https://www.aqistudy.cn/
[62] Y. Xi, Y. Zhang, and S. Ding, "Visual question answering model based on visual relationship detection," *Signal Process., Image Commun.*, vol. 80, Feb. 2020, Art. no. 115648.
[63] S. Ding, S. Qu, and Y. Xi, "Stimulus-driven and concept-driven analysis for image caption generation," *Neurocomputing*, to be published, doi: 10.1016/j.neucom.2019.04.095.
[64] S. Ding, S. Qu, Y. Xi, A. K. Sangaia, and S. Wan, "Image caption generation with high-level image features," *Pattern Recognit. Lett.*, vol. 123, pp. 89–95, May 2019.
[65] H. Liu, K. Huang, Y. Yang, H. Wei, and S. Ma, "Real-time vehicle-to-grid control for frequency regulation with high frequency regulating signal," *Protection Control Mod. Power Syst.*, vol. 3, no. 3, pp. 141–148, 2018.

SICHENG PENG received the B.S. degree from the School of Electrical Engineering, Wuhan University, in 2015. He is currently pursuing the Ph.D. degree in electrical engineering with Wuhan University, Wuhan, China. His research interests include the energy internet, regional integrated energy systems, and environment-friendly dispatch.

HONGXIA WANG received the B.S. degree in electrical engineering and automation from the Hefei University of Technology, in 2018. She is currently pursuing the master's degree with the School of Electrical Engineering and Automation, Wuhan University. Her research interests include big data, random matrix theory, and data fusion.

YUQIONG ZHANG received the Ph.D. degree from Tsinghua University, Beijing, China, 2016. She is currently a Research Staff with the China Electric Power Research Institute. Her primary research interests include energy systems and energy strategy, control of thermal systems, and science and technology project management.

DICHEN LIU is currently a Professor with the School of Electrical Engineering and Automation, Wuhan University, Wuhan, China. His current researches include power system operation and control such as low frequency oscillation, nuclear power, and system stability assessment.

JINCHANG LI received the B.S. degree in electrical engineering and automation from Wuhan University, in 2017. He is currently pursuing the master's degree with the School of Electrical Engineering and Automation, Wuhan University. His research interests include heat and electricity coordinated dispatch and integrate demand response.

HENGRUI MA received the Ph.D. degree in power system and automation from the School of Electrical engineering, Wuhan University, Wuhan, China, in 2018. He is currently a member of the Tus-Institute for Renewable Energy, Qinghai University, Xining, China. His research interests include power system transient stability analysis, regional integrated energy system, and energy storage system.